Version of Record at: https://doi.org/10.1126/sciadv.ade3186

CANCER

Dynamic bioinspired coculture model for probing ER$^+$ breast cancer dormancy in the bone marrow niche

Lina Pradhan[1], DeVonte Moore[2]†, Elisa M. Ovadia[1]†, Samantha L. Swedzinski[3], Travis Cossette[4], Robert A. Sikes[5], Kenneth van Golen[5], April M. Kloxin[1,3]*

Late recurrences of breast cancer are hypothesized to arise from disseminated tumor cells (DTCs) that reactivate after dormancy and occur most frequently with estrogen receptor–positive (ER$^+$) breast cancer cells (BCCs) in bone marrow (BM). Interactions between the BM niche and BCCs are thought to play a pivotal role in recurrence, and relevant model systems are needed for mechanistic insights and improved treatments. We examined dormant DTCs in vivo and observed DTCs near bone lining cells and exhibiting autophagy. To study underlying cell-cell interactions, we established a well-defined, bioinspired dynamic indirect coculture model of ER$^+$ BCCs with BM niche cells, human mesenchymal stem cells (hMSCs) and fetal osteoblasts (hFOBs). hMSCs promoted BCC growth, whereas hFOBs promoted dormancy and autophagy, regulated in part by tumor necrosis factor–α and monocyte chemoattractant protein 1 receptor signaling. This dormancy was reversible by dynamically changing the microenvironment or inhibiting autophagy, presenting further opportunities for mechanistic and targeting studies to prevent late recurrence.

INTRODUCTION

Prolonged burden and spread of metastatic cancer to the bone is a leading cause of fatalities associated with breast cancer (*1*–*3*). Methods for detection and treatment of breast cancer are improving and show promise in the eradication of cancer cells through targeted modes of action against endogenous aberrant intracellular survival and proliferative machinery. However, these therapies often fall short in treatment of metastatic disease because of complexities within the cancer metastatic cascade that have yet to be fully understood (*4*–*6*). In particular, a heterogeneous subpopulation of both proliferative and nonproliferative disseminated tumor cells (DTCs) survive the metastatic cascade through sustained tumor homeostasis or entrance into a period of long-term quiescence or dormancy, where dormant micrometastases or single cells often are observed in bone marrow (BM) aspirates yet remain challenging to detect with noninvasive screening (*5*, *7*). Late recurrence (after 5 or more years) has been observed predominately with estrogen receptor–positive (ER$^+$) breast cancer primary tumors, with more than 50% of late recurrences happening in the bone clinically (*8*–*10*). These late recurrences are thought to arise from dormant DTCs that survived as single cells or micrometastases and over time are stimulated by local cell-microenvironment interactions to reactivate and recommence growth (*11*, *12*). Research to date has revealed a tumor-supportive role of the local bone and BM microenvironments in cancer dormancy (*13*–*16*) [e.g., DTC direct interactions with structural extracellular matrix (ECM) proteins (*17*) or niche cells (*18*)]. Yet, clinical challenges remain in detecting dormant DTCs and targeting them for treatment (*19*, *20*). Human model systems are needed to deconstruct the complex microenvironmental factors that regulate cancer dormancy and reactivation, elucidate mechanisms of survival, and identify effective targeted therapeutics to prevent late recurrence (*21*).

Several in vitro cancer model systems with different levels of complexity have been used to study cell-microenvironment interactions in breast cancer cell (BCC) dormancy within the bone or BM niche, from traditional two-dimensional (2D) culture on ECM-coated plates to 3D culture in harvested or engineered ECMs (*22*, *23*). These models are commonly inspired by or benchmarked against animal models in vivo. Studies with these systems have demonstrated the importance of specific BCC interactions with the local BM microenvironment (*6*, *15*, *16*). For example, in 2D culture, ER$^+$ BCCs were induced into dormancy in the presence of soluble factor basic fibroblast growth factor 2 (FGF2) and sustained through survival signaling with binding to fibronectin, a constitutive ECM protein found within the BM (*24*). Furthermore, BCCs cultured in 3D-harvested ECMs, such as basement membrane extract (BME) (*25*) or decellularized tissues (*26*, *27*), exhibited dormancy and reactivation in response to specific structural proteins [e.g., incorporation of collagen or fibronectin in BME to reinitiate growth and proliferation (*28*) or secretion of thrombospondin within the perivascular niche (*19*)]. In another study, ER$^+$ BCCs cultured in BME were induced into reversible dormancy and remained in cell cycle arrest, exhibiting elevated nuclear expression of p16 and p27, until stimulated to proliferate in the presence of collagen or fibronectin ECM proteins. These dormant cells were also autophagic and sensitive to treatment with hydroxychloroquine (HCQ), suggesting autophagy as a survival mechanism that can be targeted for dormancy therapeutic intervention (*25*, *28*). Tunable engineered substrates with physiologically relevant mechanical properties also have been developed for interrogating the influence of specific ECM interactions on dormancy, where such systems provide accessibility and afford limited batch-to-batch variation of further relevance for therapeutic screening (*22*, *23*). For example, with substrates where structural niche proteins can be added individually or in combination, ER$^+$ BCCs deposited a highly fibrillar fibronectin

[1]Department of Chemical and Biomolecular Engineering, University of Delaware, Newark, DE 19716, USA. [2]Department of Chemistry and Biochemistry, University of Delaware, Newark, DE 19716, USA. [3]Department of Materials Science and Engineering, University of Delaware, Newark, DE 19716, USA. [4]Office of Laboratory Animal Medicine, University of Delaware, Newark, DE 19716, USA. [5]Department of Biological Sciences, University of Delaware, Newark, DE 19716, USA.
*Corresponding author. Email: akloxin@udel.edu
†These authors contributed equally to this work.

matrix, facilitated by transforming growth factor–β2 (TGF-β2) signaling and Rho kinase (ROCK)-generated tension, and survived in sustained dormancy through binding and attachment via $\alpha_5\beta_1$ and $\alpha_v\beta_3$ integrins, where matrix metalloproteinase 2 (MMP2) activity liberated dormant cells to become proliferative (*29*). Moving into three dimensions with a reductionist BM-inspired synthetic ECM, we previously observed sustained long-term dormancy (>5 weeks) of ER^+ BCCs in 3D monoculture (*30*). These well-defined culture systems provide opportunities for probing cell-cell interaction in addition to cell-ECM interactions.

The importance of direct cell-cell communication between BCCs and resident niche cells within the BM microenvironment has been examined in several dormancy studies. For example, a 3D hanging drop coculture of ER^+ BCCs directly with BM mesenchymal stem/stromal cells (MSCs) formed cancer spheroids and MSCs were internalized and ingested, promoting BCC survival while also suppressing tumorgenicity and suggesting entrance into dormancy (*31*). In a complementary study, ER^+ BCCs directly cocultured with different combinations of niche cells within harvested collagen-based scaffolds exhibited dormancy or persistent growth. Specifically, MSCs provided a "supportive" niche for BCC growth, whereas a combination of osteoblasts, endothelial cells, and mesenchymal cells of BM origin (HS-5s) provided an "inhibitory" niche, suggesting niche cell importance although not allowing parsing of specific cell-cell interactions (*32*). These studies where BCC and niche cells are mixed and cultured in the same construct are known as direct cocultures, where BCCs and niche cells can have dynamic and complex interactions that regulate their responses over long culture times (e.g., changing densities and distances between different cell types, competition for space, direct contact, and exchange of different types of secreted factors). Given this complexity, a few studies have examined the importance of interactions between BCCs and resident BM niche cells in dormancy through secreted soluble factor signaling. For example, in short-term 2D studies, dormant ER^+ BCCs stimulated stromal cell secretion of inflammatory cytokines, interleukin-6 (IL-6) and IL-8, which in turn stimulated a switch in dormant cell phenotype from epithelial to mesenchymal and reactivated the once dormant cells to proliferate (*12*). Moving to indirect 2D cocultures, BCC and niche cells can be cultured in separate wells connected by a membrane or with condition media periodically exchanged: For example, it was observed that ER^+ BCC growth and proliferation was suppressed when treated with the conditioned media of "educated" osteoblast cells, suggesting the relevance of secreted factor exchange between BCC and BM niche cells in dormancy induction (*33*, *34*). While studies to date demonstrate the importance of specific cell-ECM and cell-cell interactions in the BM microenvironment for inducing dormancy/growth, longer-term studies (>2 weeks) remain challenging (e.g., over growth of scaffolds by different cell types) and are needed for examining late recurrence of ER^+ BCs. Furthermore, examining the effects of soluble proteins (e.g., growth factors and cytokines) and other factors secreted from specific niche cell types in 3D culture is limited, owing in part to direct cocultures where different cell types are mixed together (*35*, *36*). Consequently, despite their potential importance, currently less is known about how soluble secreted factors exchanged between BCCs and niche cells influence dormancy and reactivation.

Model systems capable of long-term indirect coculture in 3D physiologically relevant microenvironments, informed by and benchmarked against in vivo data, are needed for probing the dynamic indirect interactions between BCCs and niche cells in dormancy and reactivation and elucidating mechanistic targets. To address this need, we first examined ER^+ BCC dormancy within an in vivo model system, where dormant DTCs were observed to be localized within the BM near the bone lining among other BM locations. To study how different interactions found in this niche regulate dormancy, with a focus on soluble secreted factors, we established and used a well-defined dynamic indirect 3D coculture model of ER^+ BCCs of different metastatic potentials (luminal A T47D, ZR-75-1; luminal B BT474) with key BM niche cells [human MSCs (hMSCs) and bone lining human fetal osteoblasts (hFOBs)]. This 3D coculture system was built upon a bioinspired synthetic matrix with cell degradability and tunable biophysical and biochemical properties, which we previously have shown useful for studies of dormancy in monoculture (*30*). Differential growth and dormancy of ER^+ BCCs were observed in these indirect 3D cocultures with hMSCs or hFOBs, respectively. We hypothesized that soluble factors released within the osteoblastic niche regulated suppression of growth and induced dormancy survival and probed these with Luminex. Furthermore, we examined the reversibility of this secreted factor–induced dormancy by exchanging the microenvironment, switching of niche cell type within or withdrawing from indirect coculture, and by targeting to inhibit identified survival mechanisms. These studies demonstrate that secreted factors within the osteoblastic niche are essential in controlling ER^+ BCC dormancy and the potential for targeting them and related survival mechanisms toward preventing late recurrence.

RESULTS

Disseminated ER^+ BCCs in vivo are dormant and autophagic at the BM site

To investigate survival mechanisms used by dormant BC DTCs that colonize the BM metastatic site, we performed intracardiac injection of ER^+ T47D cells expressing green fluorescent protein (GFP) into nonobese diabetic–severe combined immunodeficient (NOD-SCID) mice and monitored them over time using an IVIS imaging system for a whole-body scan, and surviving mice with no relapse signs were euthanized after completion of 6 weeks (*19*). Dissected whole femurs, tibia, and other organs were scanned for fluorescence with IVIS (GFP, excitation, 465 to 500 nm; emission, 520 to 560 nm) to confirm the dissemination of BCCs, where treated mice showed green regions within the bones (Fig. 1, A and B, and fig. S1), and untreated mice were used to compare for negative background fluorescence. To further confirm dissemination and focusing on the BM niche, we collected GFP-T47D colonies or cells from the BM by flushing a subset of femurs with buffer and imaging the collected effluent with confocal microscopy (fig. S2). To estimate the location of DTCs within the bone, resected femurs were whole-mounted, sectioned, stained, and imaged to identify whether BC DTCs were dormant or proliferative (Fig. 1C and fig. S3). GFP-positive T47D cells residing within the BM niche, close to the bone line, were observed; these cells had entered into a dormant (Ki-67–negative) state and exhibited a marker of autophagy (LC3B-positive), a self-degradative process to balance sources of energy for cell survival (Fig. 1D). Dormant tumor colonies were found either close to the bone lining area or on endothelial locale 6 weeks after injection by histological analysis,

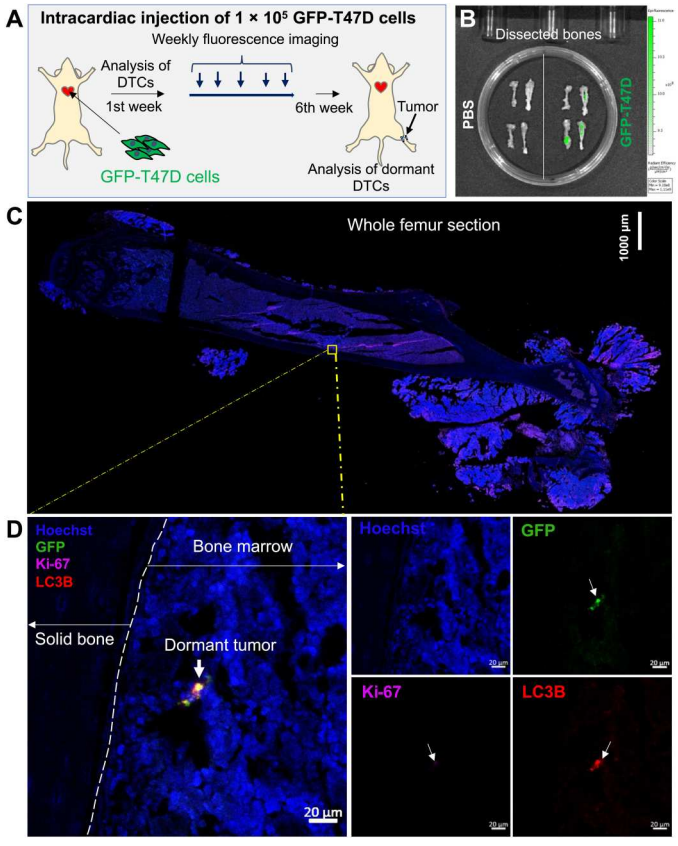

Fig. 1. ER$^+$ breast tumor cells disseminate in BM tissues in vivo (NOD-SCID mice) and exhibit dormancy and autophagy. (**A**) GFP-T47D cells were delivered through intracardiac injection, and mice (n = 5) were imaged weekly by IVIS and euthanized 6 weeks later for collection of (**B**) bone tissues for further analysis {shown here, IVIS imaging for fluorescent detection of disseminated GFP-T47D cells compared to control [intracardiac injection of phosphate-buffered saline (PBS)]}. (**C**) Representative image (tile scans of z-stack projections) of 5-µm-thick section of bone tissue; bone was sectioned, deparaffinized, and immunostained for analysis of dormant (Ki-67–negative) T47D cells (GFP, green) in the BM, where dormant tumor cells were LC3B positive (autophagy protein marker, red). Scale bar, 1000 µm. (**D**) Magnified images of region of interest within the BM tissue [yellow square in (C)], where dormant tumor cells were observed close to bone lining area (arrow marked in white). Scale bar, 20 µm. DNA was labeled with Hoechst stain (blue).

whereas untreated control mice did not bear tumors within the BM niche (fig. S4). These observations were established repeatedly with approximately one to two GFP-positive dormant small colonies per bone, few Ki-67–positive GFP-positive colonies, and no tumor growth (progression) over the time course (figs. S1 to S4). These results support the importance of the BM niche in promoting DTC dormancy and survival, where the perivascular niche within BM has previously been shown to regulate DTC dormancy (*19*). Here, our observations inspired us to examine how the lining of the bone and related niche cells and secreted factors localized within this area play a role in regulating tumor dormancy and autophagy, a potential mechanism in maintaining survival of dormant tumors (*28*, *30*, *37*).

Bioinspired in vitro indirect 3D coculture model demonstrates the importance of the BM niche in suppressing or promoting BCC growth

Despite growing knowledge that BM niche cells strongly influence tumor dormancy and activation, many of the specific interactions by which BM niche cells influence BCC function remain unclear, owing in part to in vivo microenvironment complexity (e.g., bone remodeling processes that occur with aging or injury leading to a range of dynamic cell-cell and cell-matrix interactions) (*6*, *34*). Reductionist model systems provide an opportunity to control aspects of this complexity and dissect interactions between niche cells and DTCs (*18*, *19*, *38*), with a focus to date on examining interactions between mixed populations of BCCs and niche cells in direct coculture (i.e., direct BCC–niche cell contact) (*29*–*32*, *39*, *40*). For example, direct interactions between BM niche cells and BCCs cultured in a commercial harvested collagen porous scaffold have been shown to promote BCC dormancy [coculture with human umbilical vein endothelial cells (HUVECs), BM stromal cells (HS-5s), and hFOBs] or growth (hMSCs) (*32*). Informed by our observations of dormant DTCs in vivo proximate to the bone lining, we hypothesized that soluble factors exchanged between DTCs and BM niche cells regulated BCC dormancy and set out to establish a 3D dynamic coculture model relevant for studies to examine this. Starting from an established direct coculture model system for comparison (*32*), we first separated BM niche cells (HUVECs, HS-5s, hFOBs, and hMSCs) from the BCCs (luminal A T47D), seeding each cell type into different harvested collagen scaffolds and culturing them indirectly with BCCs separated by a Transwell insert. We observed that indirect coculture with hFOBs suppressed growth of the BCCs, whereas indirect coculture with hMSCs most notably promoted continued BCC growth (figs. S5 and S6 and table S1) over 2 weeks. Note that indirect coculture with HUVECs or HS-5s alone had a limited effect on T47D growth relative to monoculture control. These observations supported the relevance of indirect BCC-hFOB interactions (e.g., soluble secreted factors) in promoting BCC dormancy, and the robust effects of indirect BCC-hMSC interactions in promoting BCC proliferation, where our continued studies focused on better understanding these interactions.

To further enhance the control of microenvironment properties and reduce variability, we next integrated a well-defined synthetic matrix within the dynamic coculture model system. The BM site is composed primarily of type I collagen and has unique matrix mechanical properties (*41*). Inspired by this collagen-rich site, a reductionist synthetic matrix was formed with relevant concentrations of (i) a bioinert multiarm macromer (PEG-4-SH, M_n ~ 20 kDa) to control the initial equilibrium swollen modulus of the matrix to be in the range of that of BM (*41*) [Young's modulus (E) ~0.6 kPa; fig. S7]; (ii) a MMP-degradable peptide linker similar to that found in collagen I to allow cell remodeling [K(alloc)G**PQ-G↓IWGQ**GK(alloc), (GPQGIWGQ)]; and (iii) an integrin-binding peptide found in collagen I for cell binding K(alloc)G$(POG)_3$PO**GFOGER**G$(POG)_4$G (GFOGER) (*30*). The hydrogel-based synthetic matrix was formed in the presence of cells using a cytocompatible step-growth thiol-ene photopolymerization affording a relatively homogenous network architecture and an optically clear material with precise control of geometry that allows the observation of homogeneous cellular responses (fig. S7) (*42*). Notably, the synthetic matrix affords facile tuning of matrix mechanical properties inspired by tissues of interest while

incorporating key biochemical cues (*30*, *42*), whereas commercially available harvested materials like the collagen scaffold often afford limited control of matrix mechanical properties or biochemical cues (*43*). Previously, we established the relevance of this synthetic matrix for long-term 3D monoculture studies of breast cancer dormancy or growth, where ER^+ BCCs were observed to exhibit limited differences in response to different integrin-binding ligands but did exhibit differential responses to matrix density. On the basis of those observations, here, a synthetic matrix composition was used that was known to be permissive to both BCC growth and dormancy (*30*, *42*). For probing cell-cell interactions and capturing more of the complexities of the BM microenvironment, we deployed the BM-inspired synthetic matrix for encapsulation and coculture of different ER^+ BCC types of increasing metastatic potential [luminal A T47D/GFP-T47D, luminal A ZR-75-1 (all data shown in electronic supplementary information), and luminal B BT474] with either hMSC or hFOB BM niche cells. BCCs in the well-defined synthetic matrix were either directly (+) or indirectly (#) cocultured with the respective BM niche cells and compared to the respective monoculture control for examining the effects of different cell-cell interactions on growth, dormancy, and survival, where dormant cells are viable, are not proliferating, and remain capable of proliferating in response to a stimulus. Cocultures were performed with the free exchange of secreted factors between cells throughout the experiment time course and in response to applied stimuli ("dynamic cocultures").

At specified times (days 1, 3, 7, 10, and 15), cell viability was assessed (live/dead staining; green fluorescence indicates live cells and red indicates dead cells, imaged with confocal microscopy) (Fig. 2, A to C, and figs. S8 to S11; S12, A and B; S13, A and B; and S14, A and B), and live cells were quantified (Volocity) (Fig. 2, D and E and figs. S12C, S13C, and S14, C and D). We observed that the ER^+ BCCs were viable (>90% viable) when cultured alone (monoculture) over 2 weeks as expected from our prior work (*30*). Divergent trends in viability were observed when BCCs were cocultured directly with BM niche cells. Consistently, high cell viability was observed within BCCs+hMSC direct coculture conditions (T47D+hMSC and BT474+hMSC, >90%), whereas slightly decreasing cell viability was observed within BCCs+hFOB direct coculture conditions (T47D+hFOB and BT474+hFOB, ~60%), where quantification analysis was executed and processed without cell separation in direct coculture conditions. Similar trends were observed for BCCs cocultured indirectly with BM niche cells over 15 days: T47D#hMSC and BT474#hMSC >90% viable and formed large clusters (Fig. 2, B and C), and T47D#hFOB and BT474#hFOB ~65% viable (Fig. 2, D and E, and figs. S12A and S13A), where the viability of each cell type could be elucidated separately. For further insights into the number of viable BCCs over time, GFP-T47D cells were used in 3D monoculture or cocultures within synthetic matrices (fig. S15) or collagen scaffolds (fig. S16). Specifically, mean fluorescence intensity (MFI) for confocal z-stack projections was analyzed as a measure of the number of viable GFP-T47D cells in 3D culture over time, an approach established by Marlow *et al.* (*32*) for studying BCC dormancy with direct cocultures. Observations with MFI over time confirmed the observations of viability made with the live/dead assay and suggested potential induction of dormancy for cocultures with hFOBs. Specifically, over time, increased MFI was observed for GFP-T47Ds in 3D monoculture and in coculture with hMSCs, indicating proliferation, whereas relatively flat, low MFI over time was observed in 3D coculture with hFOB cells with a slight decrease at day 15, suggesting viable cells with limited proliferation and some cell death. Changes in the cell density over time also can be observed with larger clusters of BCC forming in non-hFOB conditions, leading to increased proximity among cells including niche cells with BCCs in direct cocultures.

Cell metabolic activity (AlamarBlue), an indirect assessment of cell number (proliferation) and viability, was also examined in parallel (Fig. 2, F and G). The indirect coculture approach facilely permits the assessment of BCC metabolic activity separately from that of the niche cells, whereas metabolic activity for direct coculture is an aggregate response from the mixed population of BCC and niche cells. In the case of BCCs indirectly cocultured with hMSC cells, metabolic activity of BCCs was substantially enhanced over 15 days of culture in comparison to either BCC monoculture (T47D, BT474, and ZR-75-1) or indirect coculture with hFOB cells (T47D#hFOB, BT474#hFOB, and ZR-75-1#hFOB). Direct coculture of BCCs with hMSCs showed lower metabolic activity over time (T47D+hMSC, BT474+hMSC, and ZR-75-1+hMSC) as compared with indirect coculture of BCCs with hMSCs (T47D#hMSC, BT474#hMSC, and ZR-75-1#hMSC) (Fig. 2, F and G, fig. S14E, and table S2). Notably, these observations suggested increased stimulation of BCC growth through indirect cell-cell interactions (i.e., cell-secreted factors within the conditioned media as opposed to direct cell-cell contact). In contrast, flattening of metabolic activity was observed over time in either direct or indirect coculture conditions with hFOB (BCC+hFOB or BCC#hFOB), suggesting limited growth of BCCs in the presence of hFOBs. These observations suggested an entrance of BCCs into a state of dormancy, where cells exhibit minimal changes in metabolic activity, remain viable, are nonproliferative, and capable of reproliferating upon stimulation. Similar trends of metabolic activity were noticed among all types of ER^+ BCCs examined and were consistent with qualitative observations of cell morphology/cluster size (figs. S5, S6, S12 to S14, S17, and S18) and cell number (fig. S18). Together, these data recommend that ER^+ BCC growth or inhibition of growth depends on BM niche cell type and the varying submicroenvironments that they provide. Note that indirect coculture, where niche cells and BCC are cultured in separate 3D matrices, also allows facile assessment of the niche cell growth and viability. hMSCs indirectly cocultured with BCCs sustained high viability and proliferation (T47D#hMSC, BT474#hMSC, and ZR-75-1#hMSC) (>85% viability over 15 days; figs. S12C, S13C, and S14D). hFOBs indirectly cocultured with BCCs exhibited viability and some initial growth followed by a decrease in cell viability while maintaining cluster diameter at later time points (figs. S12, C and D, S13C, and S14C). Overall, from these data and observations, we hypothesized that secreted factors associated with hFOBs play a primary role in BCC dormancy and hMSCs influence BCC growth with a potential role in dormant BCC reactivation.

BM niche cell induction of ER^+ BCC dormancy and reactivation elucidated with dynamic indirect 3D coculture

To further investigate the potential for ER^+ BCC dormancy and activation in a BM microenvironment–dependent manner, ER^+ BCC proliferation (T47D, BT474, and ZR-75-1) was evaluated using a 5-ethynyl-2′-deoxyuridine (EdU) assay within 3D indirect cocultures and compared to monoculture controls. BCCs were pulsed with

Version of Record at: https://doi.org/10.1126/sciadv.ade3186

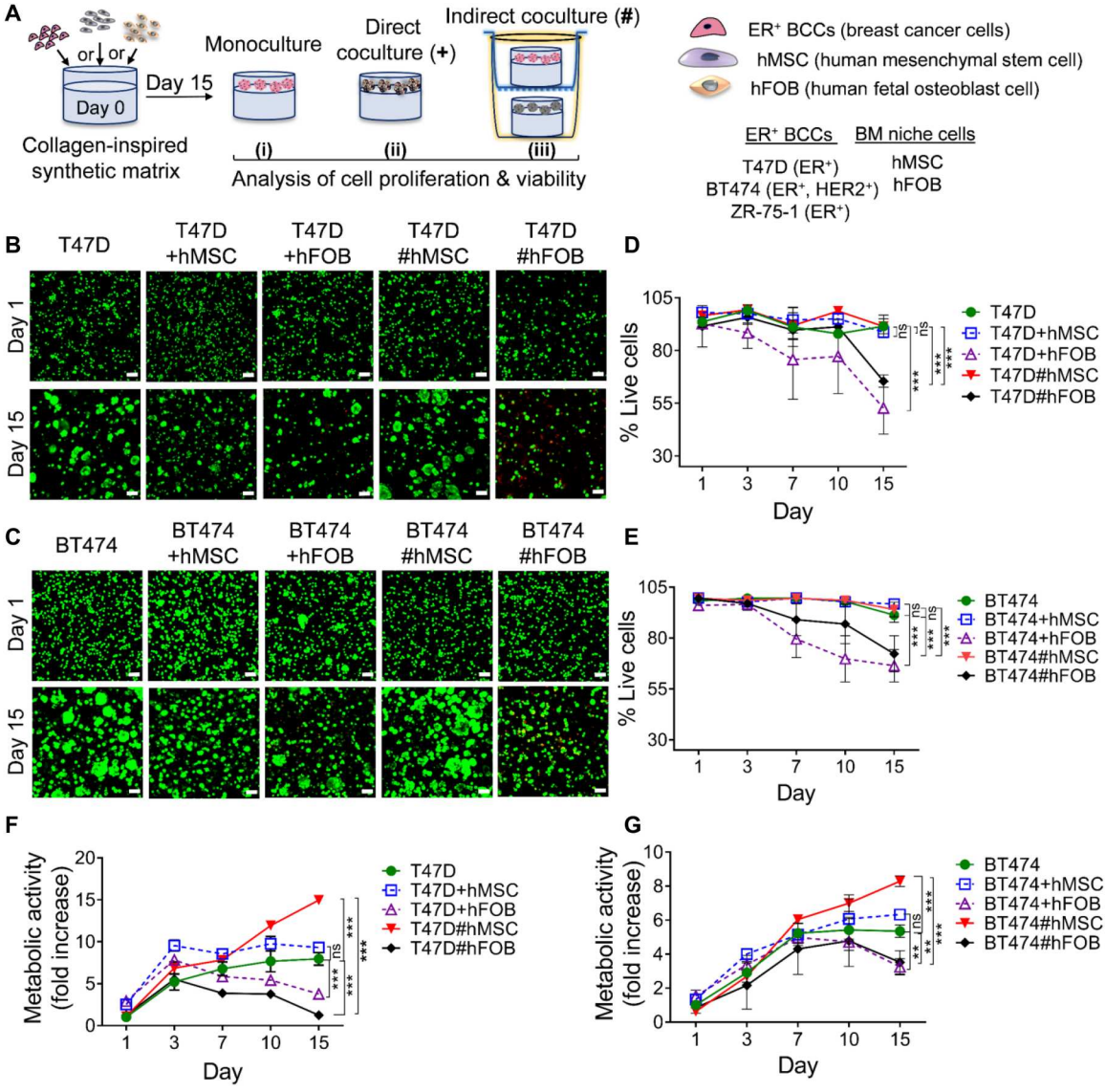

Fig. 2. Assessment of viability and metabolic activity of ER$^+$ BCCs in 3D direct and indirect in vitro coculture over time. (**A**) Approach for direct and indirect 3D coculture of BM niche cells (hMSC or hFOB) with BCCs using synthetic matrices in multiwell or Transwell plates. (**B** and **C**) Representative images for assessment of BCC response in synthetic matrices (viability) for luminal A T47D or luminal B BT474 alone (growth control), in direct coculture (+) or in indirect coculture (#) (confocal z-stack projections; live cells were stained green, and dead cells were stained red). Scale bars, 100 μm. (**D** and **E**) Quantitative analysis of viable cells. (**F** and **G**) Metabolic activity over time (fold change relative to day 1 for each condition). Significant differences were assessed by one-way analysis of variance (ANOVA) with Tukey's multiple comparisons test, where differences are shown for comparison between various conditions at day 15 time point (**P < 0.01, ***P < 0.001; not significant (ns); full set of P values for other comparisons can be found in table S2). Similar data were obtained for luminal A ZR-75-1 (fig. S6). Larger versions of representative images with channels split are available in the electronic supplementary information (ESI) (figs. S8 to S11). Data shown represent the means ± SD (n = 3).

EdU at time points of interest during culture and fixed and stained with AF647 (magenta) for identification of EdU-positive (EdU^{+ve}) proliferating cells (S phase) among all cells with Hoechst-stained nuclei (DNA, blue) (Fig. 3, A and B, and figs. S17, A to C, and S19 to S24). A few to no BCCs indirectly cocultured with hFOBs were observed to be proliferating at day 15 in 3D culture (<1% EdU^{+ve} BCCs; Fig. 3, C and D, and fig. S17D). In the context of prior sustained viability and metabolic activity observations (Fig. 2 and fig. S15), these data support that BCCs were no longer proliferating but were alive, an indication of dormancy. In contrast, a large number of EdU^{+ve} cells were observed when BCCs were indirectly cocultured with hMSCs and statistically higher than BCC in monoculture (>40% versus >25% EdU^{+ve} BCCs, respectively) or hFOB coculture. Furthermore, additional samples were stained for the proliferation marker Ki-67 (a nuclear protein expressed during the cell cycle), imaged by confocal microscopy, and quantitatively analyzed (fig. S18). Similar trends and percentages of proliferative cells (Ki-67^{+ve}) were observed in all conditions. To better understand BCC growth or growth arrest (dormancy), respectively, we performed cell cycle analysis (fig. S25). T47Ds were isolated from 3D monoculture or indirect 3D coculture with hFOBs or hMSCs on days 1 and 15, and cell cycle analysis was performed

Version of Record at: https://doi.org/10.1126/sciadv.ade3186

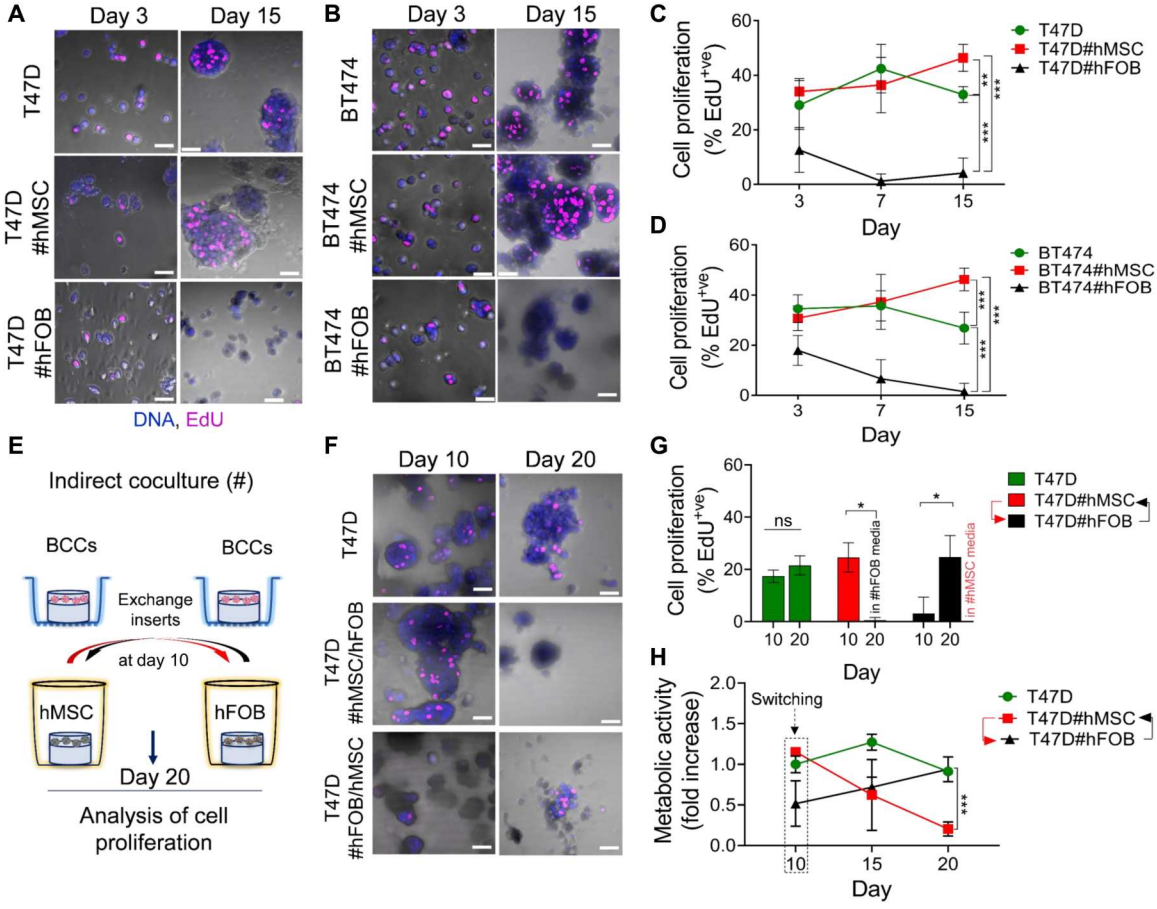

Fig. 3. Probing effects of BM niche secreted factor on BCC dormancy with dynamic indirect 3D cocultures. BCC proliferation assessment of over time in different 3D culture conditions using EdU assay. (**A** and **B**) Representative images of T47Ds and BT474s showing EdU^{+ve} cells at days 3 and 15 in monoculture (control) or indirect coculture (#); EdU (magenta), Hoechst (blue); confocal z-stack projections. Scale bars, 50 μm. (**C** and **D**) Quantification of EdU^{+ve} T47D and BT474 cells (**$P < 0.01$, ***$P < 0.001$; table S3). (**E**) Schematic of approach for assessment of BCC dormancy/reactivation for T47D in monoculture or indirect coculture with an exchange of Transwell inserts between different BM niche cells (hFOB or hMSC) at day 10. (**F**) Representative images of BCC during insert exchange study using EdU proliferation assay [confocal z-stack projections; F-actin (green), DNA (blue), EdU (magenta)]. Scale bars, 50 μm. (**G**) Quantitative analysis of EdU^{+ve} T47D cells after insert exchange. Significant differences were assessed by Student's two-sided *t* test, where differences are shown for comparison between time points in mono- and coculture conditions. (**H**) Metabolic activity assessment before and after insert exchange on day 10 (AlamarBlue assay, fold change relative to day 3 for each condition). Statistical differences were determined by ANOVA with Tukey's multiple comparisons test (*$P < 0.05$, ***$P < 0.001$; tables S3 and S5). Data shown represent the means ± SD ($n = 3$). Larger versions of representative images with channels split are available in the ESI (figs. S19 to S24).

with flow cytometry (fig. S25), confirming cell cycle arrest (G_1 population) or induction of cell death (sub-G_0 population) for BCCs in coculture with hFOBs. These differences in cell cycle further support the observations of BCC dormancy or growth made with viability (Fig. 2 and fig. S15), metabolic activity (Fig. 2), and EdU and Ki-67 assays (Fig. 3 and fig. S8). Overall, these data support the importance of BM niche cells (hMSCs or hFOBs) in BCCs growth or dormancy, respectively.

To further probe dormancy and the potential for reactivation, we established an approach for assessing BCC response to changes in the BM microenvironment with Transwell insert exchange (Fig. 3E). Specifically, we examined the reactivation of dormant BCCs by switching from the dormancy-promoting osteoblastic (BCC#hFOB) niche into the growth-promoting (BCC#hMSC) niche at day 10 and assessed proliferation and viability. Day 10 was selected for the switch on the basis of observations of dormancy in osteoblastic indirect coculture (BCC#hFOB) and increased growth in the stem cell indirect coculture (BCC#hMSC) (Figs. 2 and 3, A to D, and figs. S15 and S25). A notable percentage of EdU^+ cells and increasing metabolic activity were observed after switching dormant BCCs into either the growth-promoting hMSC microenvironment or growth media, indicating reactivation from dormancy (Fig. 3, F to H, and figs. S26 and S27, A and B). Similarly, proliferating BCCs were switched from the growth-promoting (BCC#hMSC) niche to the dormancy-promoting osteoblastic (BCC#hFOB) niche at day 10, and a substantial decrease in proliferation and metabolic activity was observed. These exciting observations further supported BCC dormancy within the osteoblastic niche and the importance of indirect interactions (e.g., soluble factors) in regulating BCC dormancy and reactivation, as well as an innovative tool for studying reactivation from dormancy for further mechanistic and targeting studies.

Dormant ER$^+$ BCCs are autophagic, as observed in vivo, with the ability to recommence proliferation upon changes in the microenvironment

We next sought to benchmark the in vitro model system versus our in vivo observations, as well as literature reports, by investigating autophagy as a potential targetable mechanism of cell survival in dormancy (*31*, *37*). As noted earlier, autophagy is a process by which cells survive under metabolic stress by degrading organelles and cytosolic protein to conserve energy through fusion of lysosomes for recycling dysfunctional organelles. To probe this, we analyzed the expression of the microtubule-associated LC3B protein, a central protein in the autophagy pathway that is used for autophagosome detection and considered a positive marker for autophagy, over time in BCCs indirectly cocultured with niche cells or in monoculture over 15 days (Fig. 4 and figs. S28 to S32). BCCs showed increased LC3B^{+ve} puncta (>50% of the cells) when cocultured with dormancy-promoting hFOBs (T47D#hFOB and BT474#hFOB), whereas no LC3B^{+ve} cells were observed when cocultured with growth-promoting hMSCs (T47D#hMSC and BT474#hMSC) (Fig. 4, A to D, and fig. S32, A and B).

We hypothesized that the high levels of autophagy observed from BCCs indirectly cocultured within the dormancy-promoting hFOB niche could be reversed upon switching to growth-promoting hMSC niche. To test this, we exchanged the Transwell inserts of BCCs between dormancy-promoting and growth-promoting indirect coculture microenvironments on day 10 in 3D culture, which was shown to promote reactivation from dormancy (Fig. 3), and analyzed for LC3B expression (Fig. 4, E to G, and fig. S32, C and D). A substantial increase in the percentage of BCCs with LC3B^{+ve} puncta was observed when BCCs cocultured with growth-promoting hMSCs were transferred into coculture with dormancy-promoting hFOBs at day 10 (from 0 to >45% LC3B^{+ve} BCC with

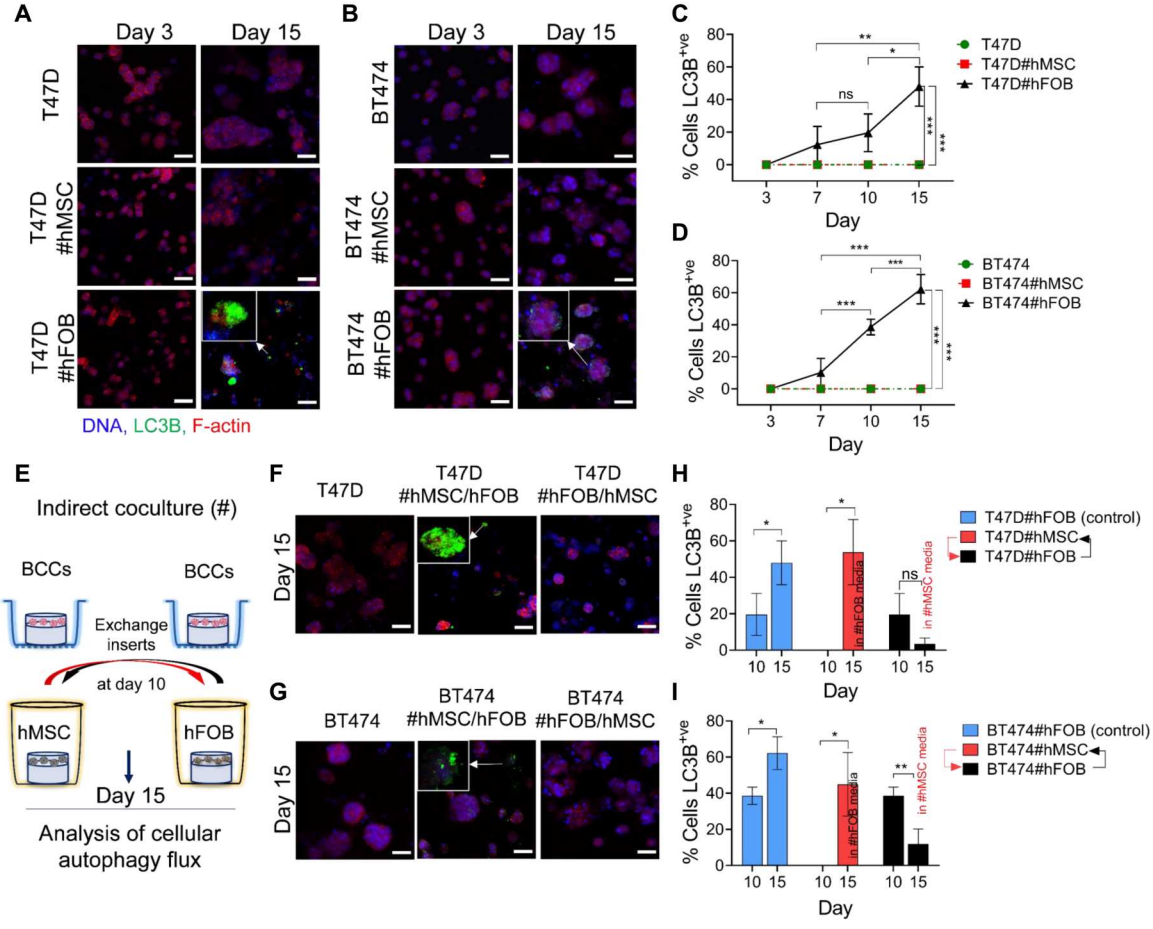

Fig. 4. BCCs exhibit reversible induction of autophagy with dormancy and reactivation in dynamic 3D indirect coculture. (**A** and **B**) Immunofluorescent staining of autophagic protein (LC3B), F-actin (phalloidin), and DNA (Hoechst) of T47D and BT474 cells in 3D culture, with # denoting Transwell indirect coculture [representative confocal z-stack projections; F-actin (red), LC3B^{+ve} puncta (green), DNA (blue)]. Scale bars, 50 μm. (**C** and **D**) Quantitative analysis of cells positive for LC3B^{+ve} puncta. Significant differences were assessed by ANOVA with Tukey's multiple comparisons test, where differences are shown for comparison between multiple conditions at day 15 time point (*P < 0.05, **P < 0.01, and ***P < 0.001). (**E**) Schematic representation of switching microenvironment by insert exchange between two different coculture conditions with T47D cells at day 10 and continued observation up to day 15 (T47D#hMSC/hFOB and T47D#hFOB/hMSC). (**F** and **G**) Representative images (confocal z-stack projections). Scale bars, 50 μm. (**H** and **I**) Quantitative analysis of BCCs with LC3B^{+ve} puncta for T47D (H) and BT474 (I) cells after insert exchange. Significant differences were assessed by Student's two-sided t test, where differences are shown for comparison between time points in coculture conditions (*P < 0.05, **P < 0.01). A full set of P values can be found in table S6. Data shown represent the means ± SD (n = 3). Larger versions of representative images with channels split or enlarged regions of interest are available in the ESI (figs. S28 to S32).

BCC#hMSC➔BCC#hFOB; denoted as BCC#hMSC/hFOB). Similar LC3B^{+ve} expression was observed for BCC#hMSC/hFOB to BCCs in continuous coculture with hFOB cells (Fig. 4, H and I). Few LC3B^{+ve} BCCs were observed when BCCs cocultured with dormancy-promoting hFOBs were transferred into coculture with growth-promoting hMSCs on day 10 (~10% LC3B^{+ve} BCC with BCC#hFOB➔BCC#hMSC; denoted as BCC#hFOB/hMSC), indicating resolution of autophagy during reactivation of dormant cells. Overall, these findings suggested that hMSC indirect coculture minimized autophagy induction in BCCs, and nonproliferative dormant BCCs can recommence proliferation after switching microenvironments. These observations support the involvement of soluble factors secreted into the media during indirect coculture that may effectively promote the dormancy and reactivation of BCCs.

High levels of pivotal secreted bioactive proteins observed in dormancy-promoting osteoblastic niche cocultures

We hypothesized that soluble factors, particularly bioactive proteins, released within the osteoblastic niche regulated the suppression of growth and induced dormancy survival. To probe this within the model system and identify potential targets for regulating dormancy, we selected a range of bioactive proteins known to be pivotal in the metastatic cascade including cell growth, migration, survival, and death [TNFα (tumor necrosis factor–α), MCP1 (monocyte chemoattractant protein 1), FGF2, IL-6, MMP1, and VEGF-A (vascular endothelial growth factor A), and EGF (epidermal growth factor)] (*34*, *44*–*49*) and performed a Luminex assay to determine the level of these secreted cytokines, growth factors, enzyme, and chemokines presented within conditioned media from dormancy-promoting hFOB cocultures or growth-promoting hMSC cocultures with BCCs. High levels of TNFα, MCP1, FGF2, and IL-6 were observed in BCC#hFOB coculture–conditioned media in comparison to BCC monoculture and BCC#hMSC-conditioned media, whereas high levels of MMP1 and VEGF-A were observed in BCCs#hMSC-conditioned media in comparison to BCCs monoculture and BCCs#hFOB, assayed at day 10 culture, and normalized to the untreated growth media (Fig. 5, A and B, and fig. S33). Day 10 was selected for this analysis as it was observed as the "tipping point" for conclusive induction of dormancy (cells viable, not proliferating, and capable to recommencing proliferation) and maintenance of overall viability of BCCs in 3D coculture with hFOBs based on metabolic activity, live/dead, EdU, Ki-67, GFP, and cell cycle assays. These observations, in conjunction with our earlier observations of dormancy/reactivation, suggested that these specific bioactive proteins (TNFα, MCP1, FGF2, and IL-6) at moderate to high levels, among other factors, could be pivotal in regulating BCC dormancy. Similarly, a high level of MMP1 and VEGF-A proteins could be regulating BCC growth.

TNFR1 and CCR2 blocking promotes and TNFα and MCP1 treatment suppresses BCC growth

To further investigate the mechanism of BCC dormancy within the BM niche and provide potential targets for addressing it, we designed an experimental approach to assess the effects of specific soluble factor signaling pathway inhibition or stimulation in ER^{+} BCC dormancy induction, focusing on the receptors TNR1 and CCR2 associated with inflammatory cytokines TNFα and MCP1. In general, TNFα and MCP1 have several roles directly or indirectly in inducing proliferation, survival (dormancy), and apoptosis of tumor cells (fig. S34, A and C) (*46*, *50*–*52*). Here, we selected two specific receptor antibody antagonists: an anti-TNFR1 (TNF receptor 1) antibody that binds TNFR1, blocking the Fas-associated death domain protein/tumor necrosis factor receptor type 1-associated death domain protein (TRADD) signaling cascade (fig. S34B) (*53*, *54*), and an anti-CCR2 antibody that binds CCR2, blocking the PI3K-Akt-mTOR signaling cascade (fig. S34D) (*55*). To test potential dose-dependent effects of anti-TNFR1 and anti-CCR2 either singly or in combination, a metabolic activity assay was performed on T47D cells in standard 2D culture over 48 hours (fig. S35), and an effective dose that maintained metabolic activity (2 ng ml^{-1}) was selected for subsequent use in 3D culture studies. For 3D culture studies, T47D cells were treated with blocking antibodies and then encapsulated within the synthetic hydrogel and cultured individually in monoculture or indirectly with hFOB cells in coculture as before for 15 days while supplementing media with antibodies to maintain blocking (Fig. 6A). Within the T47D#hFOB coculture condition, anti-TNFR1 and anti-CCR2 singly or in combination induced proliferation and enhanced the percentage of the viable cells BCCs, rescuing these BCCs from a fate of dormancy and increasing their viability relative to untreated coculture. Note that treatment of T47D cells in monoculture with anti-TNFR1 and anti-CCR2 in single and combinatory fashion did not affect their viability relative to untreated T47D cells in monoculture (Fig. 6, B and C, and fig. S36). In addition, hFOBs in treated coculture exhibited good viability and growth relative to hFOBs in untreated coculture, suggesting that the signaling associated with these receptors may play a role in the growth and viability not only of T47Ds but also of hFOBs (fig. S37). Similar trends were observed using a metabolic activity assay (Fig. 6D): A significant increase in BCC metabolic activity in coculture with hFOBs was observed with antagonist treatment by day 15, indicating BCC viability and proliferation, particularly in comparison to untreated BCCs in dormancy-promoting hFOB coculture. These observations demonstrated the importance of TNFR1 and CCR2 receptors in the induction of breast cancer dormancy in the osteoblastic niche and, in conjunction with the Luminex data, suggested the potential importance of TNFα and MCP1 signaling, as well as future opportunities for evaluation of related treatment strategies.

To assess whether BCC dormancy could be induced and maintained with these soluble factors, we encapsulated T47D cells in the hydrogel and then applied soluble TNFα or MCP1 either singly or combination (1:1 ratio; 100 ng ml^{-1} each) in growth media (Fig. 7A). T47D in monoculture with TNFα, MCP1, or TNFα + MCP1 cytokine/chemokine over time exhibited substantial growth inhibition with flat metabolic activity, qualitatively smaller cluster volumes, and decreased viability relative to untreated monoculture control (~80% relative to 95%, respectively). These observations were similar to the untreated coculture condition T47D#hFOB, suggesting cellular dormancy (Fig. 7, B and C, and fig. S38). Trends in metabolic activity were consistent with observations of cell viability over time (Fig. 7D). By 15 days, nonsignificant differences were noted between all cytokine treatment conditions and untreated coculture (T47D#hFOB). Overall, these data support the importance of specific cytokines effects on T47D growth/dormancy and highlight the utility of the innovative well-defined dynamic coculture system for mechanistic studies and the identification of potential therapeutic targets.

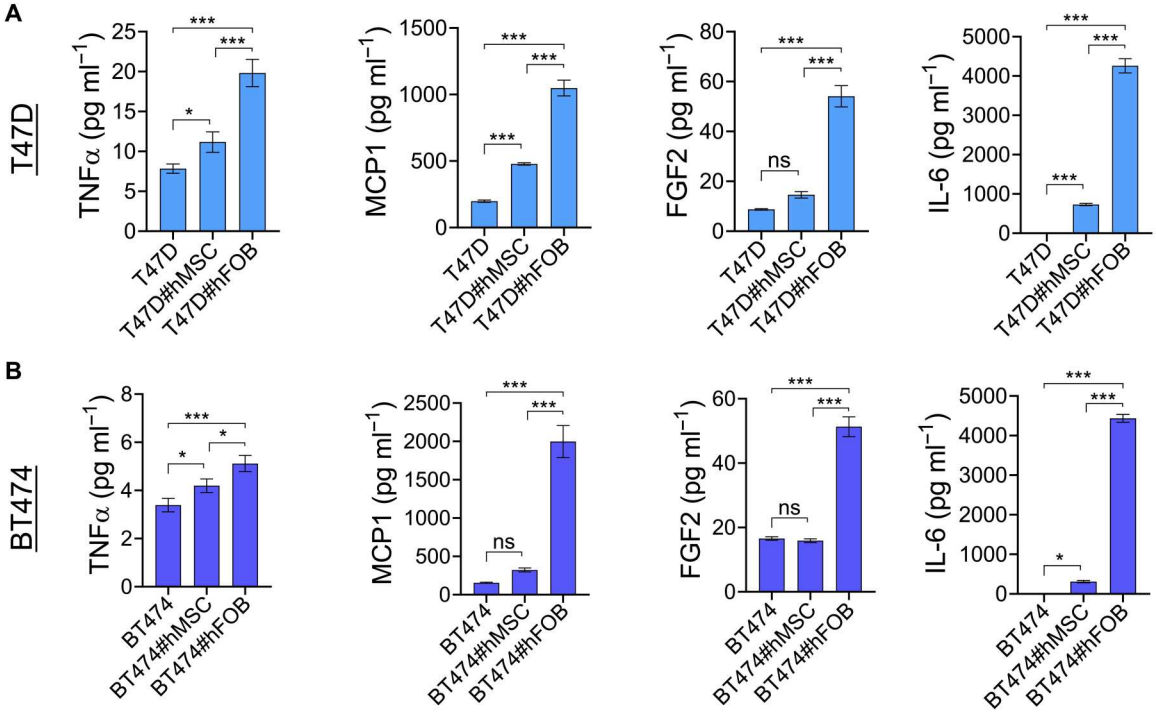

Fig. 5. Assessment of specific bioactive proteins within 3D indirect cocultures for mechanistic insights into the dormancy of BCCs. Conditioned media were collected from 3D monoculture and indirect (#) cocultures of BM niche cells (hMSC or hFOB) with BCCs (T47D or BT474) on day 10 and examined for specific cytokines with Luminex assay. The concentrations of secreted cytokines were normalized to fresh growth medium and expressed as picograms per milliliter where averages are shown for (**A**) T47D and (**B**) BT474 cells in monoculture or indirect coculture. Significant differences were assessed by ANOVA with Tukey's multiple comparisons tests, where differences are shown for comparison between multiple conditions at day 10 time point (*$P < 0.05$, ***$P < 0.001$; full set of P values can be found in table S7). Data shown represent the means ± SD ($n = 3$).

TNFR1 and CCR2 blocking prevents and TNFα and MCP1 treatment induces dormancy and autophagy of BCCs

To further assess the importance of TNFR1 and CCR2 signaling in dormancy, BCC proliferation in coculture with hFOBs with and without antagonist (anti-TNFR1, anti-CCR2, and anti-TNFR1 + anti-CCR2) was more directly assessed over time with an EdU assay (Fig. 8A) (*23*, *30*). We observed a significant increase in proliferation with a higher percentage of EdU^{+ve} T47D cells at day 15 in culture in all treated conditions (Fig. 8B) relative to untreated indirect coculture control, which as before exhibited no to few EdU^{+ve} BCC (<1%). We further stained a set of samples for autophagy marker LC3B (green) and imaged with confocal microscopy (Fig. 8C and fig. S39). Statistically, zero percent of BCCs were observed with $LC3B^{+ve}$ puncta in treatment conditions [T47D#hFOB treated with antagonist(s)], whereas the untreated T47Ds cocultured with hFOB (T47D#hFOB, control) showed a significant percentage of BCCs with $LC3B^{+ve}$ puncta (Fig. 8D). These observations indicated successful blocking of the receptors and downstream signaling pathways that induced dormancy and autophagy and importance of this signaling within the osteoblastic niche for promoting BCC dormancy and autophagy.

To directly test the impact of TNFα and MCP1 on BCC dormancy, we administered TNFα and MCP1 directly to T47D cells in monoculture over all 15 days and assessed proliferation and autophagy [EdU (magenta), LC3B (green), Hoechst (blue), phalloidin–tetramethyl rhodamine isothiocyanate (TRITC) (red), and confocal microscopy] (Fig. 9A and fig. S40). We observed that the percentage of EdU^{+ve} BCCs notably decreased, while the percentage of BCCs with $LC3B^{+ve}$ puncta increased over time, similar to trends observed in the untreated dormancy-inducing coculture condition (T47D#hFOB) (Fig. 9, B and C). While the effects of TNFα and TNFα + MCP1 were consistent over the experimental time course, a significant decrease in the percentage of proliferating cells relative to the monoculture growth control was not observed until after day 7 with MCP1 treatment, indicating a slower or delayed effect on BCCs proliferation/dormancy induction (Fig. 9B). In addition, the percentage of BCC with $LC3B^{+ve}$ puncta was significantly higher in TNFα− and TNFα + MCP1−treated conditions compared to MCP1 at day 15 (Fig. 9, C and D). Together, trends of EdU^{+ve} and $LC3B^{+ve}$ BCCs treated with TNFα and TNFα + MCP1 were most similar to untreated T47D#hFOB coculture conditions, suggesting the importance of TNFα in observations of dormancy and autophagy within the osteoblastic niche. Overall, our observations suggested that treatment with specific cytokines/chemokines suppressed T47D growth and maintained cellular dormancy, presenting targets for future investigations to target in dormancy (e.g., sustain dormancy or promote apoptosis).

Autophagy inhibition decreases the formation of $LC3B^{+ve}$ puncta in dormant BCCs and prevents the proliferation-dormancy switch

To further test the importance of autophagy in BCC dormancy within the osteoblastic niche, T47D cells were cultured in synthetic

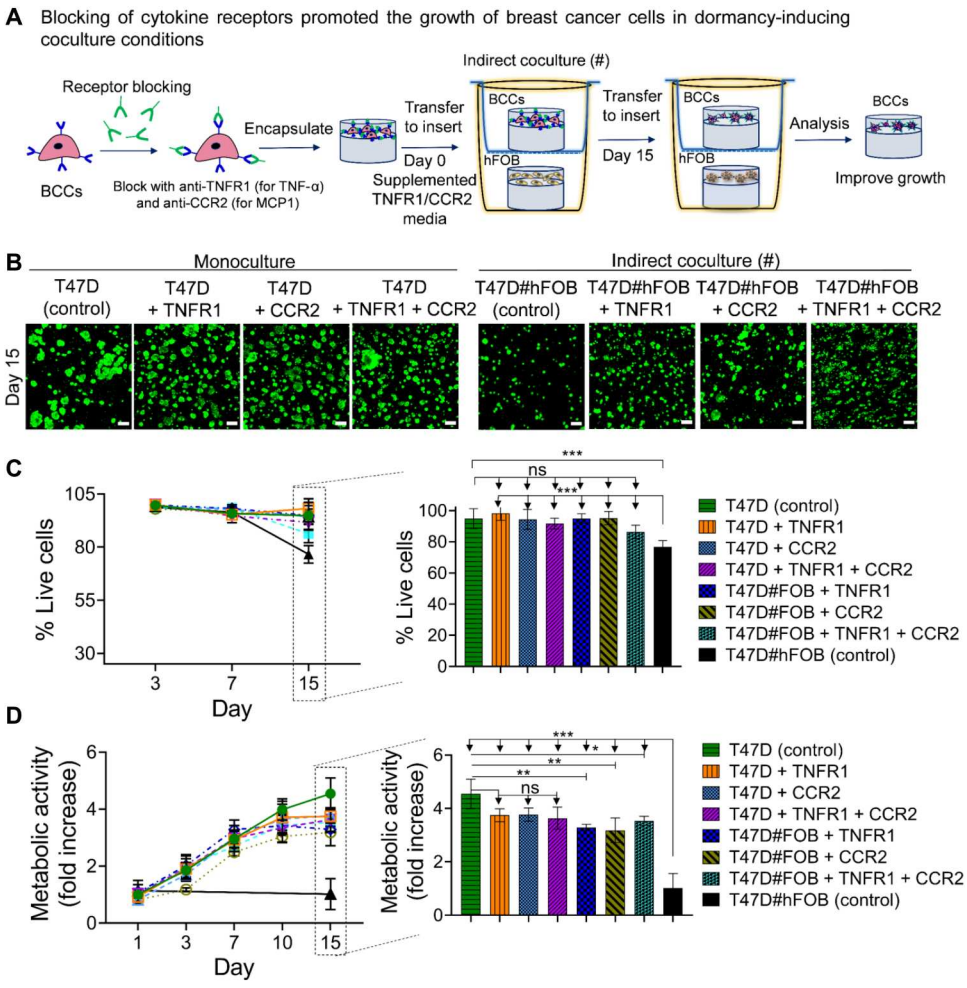

Fig. 6. Probing effects of receptors for soluble bioactive proteins on BCCs viability and growth: Antagonistic study. (**A**) Approach for probing importance of cytokine binding on the induction of dormancy and autophagy: BCCs were cultured with anti-TNFR1 and anti-CCR2 either in 3D monoculture or indirect coculture with hFOBs. (**B**) Representative images of BCCs in 3D culture (viability) after blocking of cytokine receptors for T47Ds either in monoculture or in indirect coculture with hFOBs (T47D#hFOB) as compared to untreated controls (confocal z-stack projections; live cells were stained green, and dead cells were stained red). Scale bars, 100 μm. (**C**) Quantitative analysis of viable cells over time in 3D culture, where comparisons among conditions on day 15 are represented in the bar graph on the right. (**D**) Metabolic activity over time for BCCs in 3D culture [untreated controls and treated T47Ds versus indirect (#) T47D#hFOB coculture] with a quantitative comparison of conditions on day 15 to the right (fold change relative to day 1 for each condition). Significant differences were assessed by ANOVA with Tukey's multiple comparisons test, where differences are shown for comparison between controls and multiple conditions at day 15 time point (*$P < 0.05$, **$P < 0.01$, and ***$P < 0.001$); full set of P values for other comparisons can be found in tables S9 and S10). Data shown represent the means ± SD ($n = 3$).

matrices either alone or in indirect coculture with hFOBs (T47D#hFOB) and treated with an autophagy inhibitor HCQ (12.5 μg ml^{-1}; fig. S41). The effects of the number of HCQ treatments on the timing of BCC dormancy and autophagy were evaluated in the osteoblastic niche (T47D#hFOB) and compared to T47D monoculture control (Fig. 10A). Specifically, we applied a first dose of HCQ on day 6 and to half the treated samples of a second dose on day 14. Samples were cultured for prolonged times to determine the exact time course in BCC switching from dormancy to proliferation to dormancy. For analysis, samples were fixed and stained with autophagy LC3B marker (AF488, green), cytoskeleton (phalloidin-TRITC, red), and nuclei (Hoechst, blue) and imaged with confocal microscopy.

We observed a substantial decrease (approximately 0%) in the percentage of BCCs with $LC3B^{+ve}$ puncta over the initial 20 days (from days 7 to 20) of culture when the first dose (single) of HCQ was applied to T47D#hFOB coculture condition (Fig. 10B); an increase in % $LC3B^{+ve}$ puncta cells was observed at day 25 compared to day 20, suggesting recommencing of autophagic dormancy. A complete inhibition of autophagosome formation, over the experiment time course of 25 days, was achieved with application of a second dose on day 14 (Fig. 10C and fig. S42A), suggesting successful autophagy inhibition. As before, a significant percentage of BCCs with $LC3B^{+ve}$ puncta were observed in the untreated 3D control (T47D#hFOB), indicative of continued autophagy in dormancy.

Further supporting the emergence from dormancy with HCQ treatment, the number of T47D cells in coculture increased from days 10 to 15 when treated with either a single or double dose of HCQ (treated T47D#hFOB), followed by a decrease in the

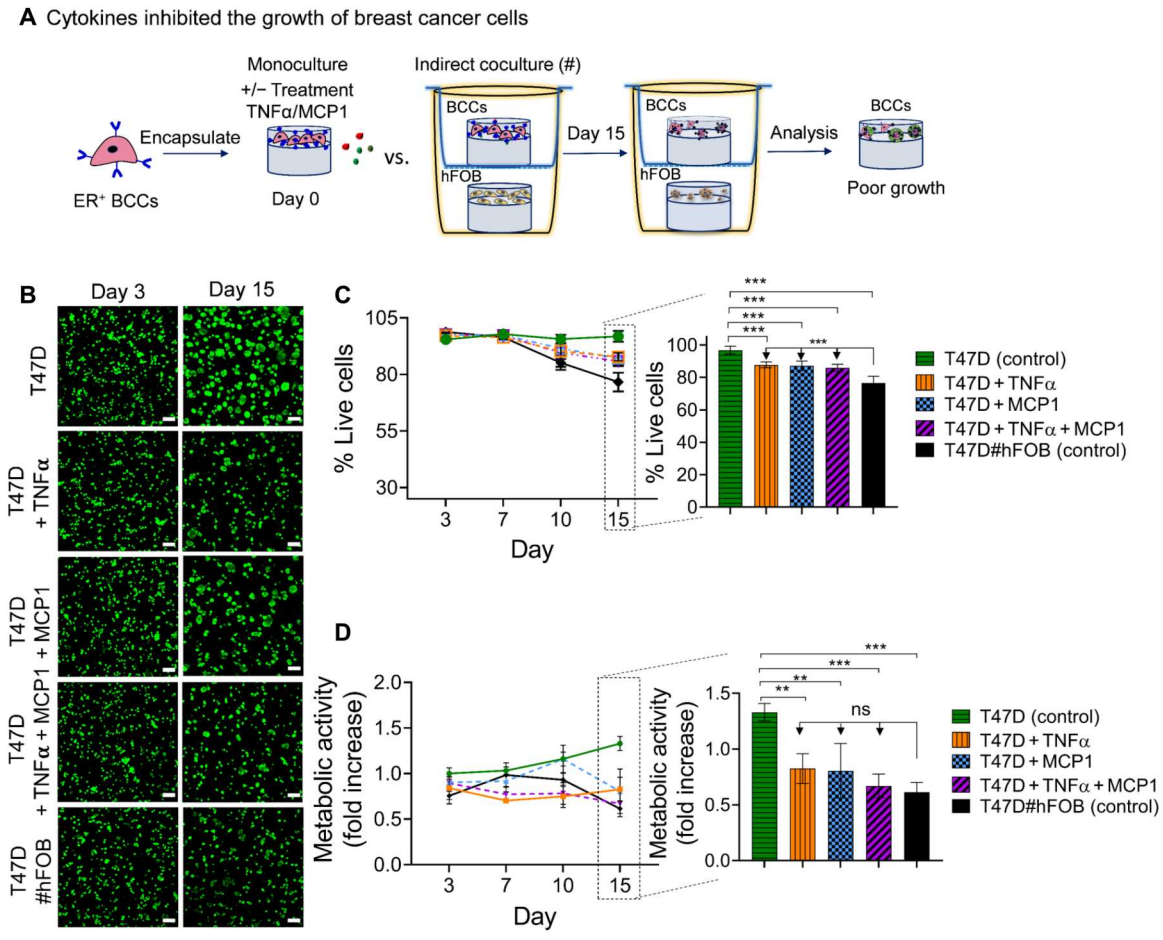

Fig. 7. Probing effects of soluble bioactive proteins on BCCs viability and growth: Cytokines study. (**A**) Schematic representation of probing effects of cytokines (recombinant human TNFα and MCP1) on the induction of dormancy and autophagy in T47D cells in 3D cultures. (**B**) Representative images of T47D cells in 3D cultures with and without TNFα and MCP1 in comparison to untreated coculture control (T47D#hFOB) or untreated T47D monoculture (further analyses available in fig. S15). (**C**) Quantitative analysis of viable cells at each time point where day 15 comparisons are shown in the bar graph on the right. (**D**) Metabolic activity at each time point where day 15 comparisons are shown in the bar graph on the right (fold change relative to day 3 for each condition). Significant differences were assessed by ANOVA with Tukey's multiple comparisons test, where differences are shown for comparison between controls and multiple conditions at day 15 time point (**$P < 0.01$, ***$P < 0.001$); full set of P values for other comparisons can be found in tables S9 and S10). Data shown represent the means ± SD ($n = 3$).

number of T47D cells (back to initial levels) after day 15, representing preliminary growth with HCQ treatment followed by limited growth and suggesting that the dose was insufficient to inhibit dormancy (Fig. 10D). However, by the end of the experiment time course (day 25), a double dose of HCQ in T47D#hFOB condition showed a significantly higher number of cells than a single-dose treatment and untreated coculture condition (T47D#hFOB as a control), suggesting longer growth with the double dose after complete inhibition of autophagosome formation. Note that no detrimental effects of HCQ doses on T47D cell growth were observed in 3D monoculture controls since T47D cells treated with and without HCQ exhibited similar increases in cell number during the experiment time course (fig. S42B).

These examinations collectively demonstrate the relevance of targeting autophagy for modulating BCC dormancy within the osteoblastic niche and that autophagy inhibition in a dormant state is sensitive to the doses of HCQ for treatment. In addition, these studies demonstrate the utility of the indirect dynamic coculture ER^+ dormancy model for both mechanistic and therapeutic strategy studies.

DISCUSSION

ER^+ breast cancer dormancy and reactivation leading to late recurrence are increasingly identified as an important clinical challenge, along with other types of metastatic disease. While several targeted therapies have improved outcomes (*2*, *9*, *56*), patients continue to suffer from relapse and metastases, a major cause of death. Clinical observations suggest that many of the patients with breast cancer have dormant DTCs in the BM in early stages of the disease, which are currently difficult to detect or target and lead to growing metastases at late times, up to decades after diagnosis and successful treatment of primary disease (*32*, *57*–*60*). Thus, there is a need to understand BCC dormancy as a mechanism for dormant DTC survival over long times that leads to late recurrence. Recent investigations suggest that the disseminated BCCs at distant metastatic sites have a limited growth period followed by the

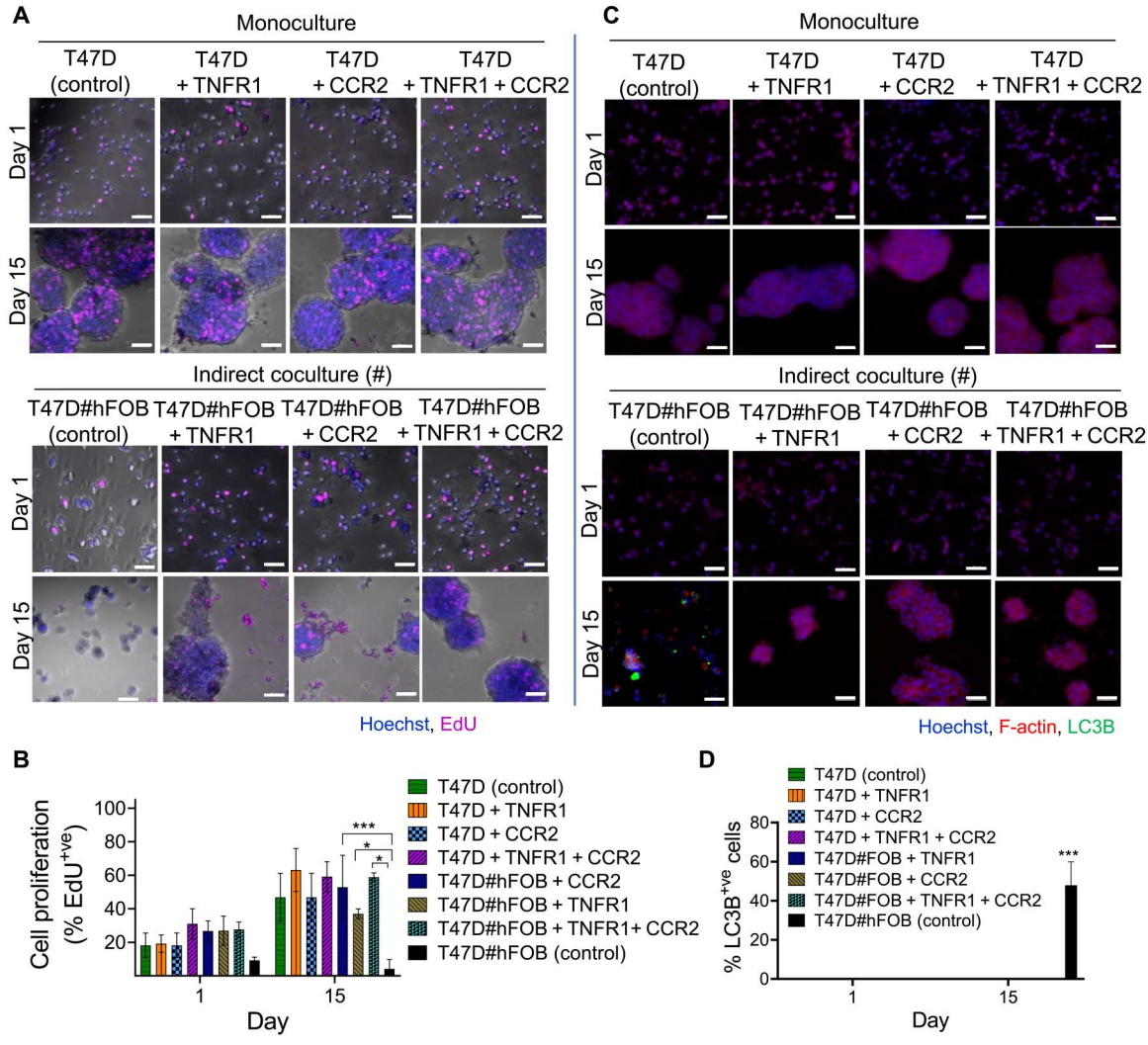

Fig. 8. Probing effects of receptors for soluble bioactive proteins on the induction of dormancy and autophagy: Antagonistic study. (**A**) BCC proliferation over time in different 3D culture conditions with and without treatment with anti-TNFR1 and anti-CCR2 was assessed with EdU proliferation assay. Representative images of T47D showed EdU^{+ve} cells at day 3 and 15 time points [untreated controls or treated monoculture and indirect cocultures (#); confocal z-stack projections; EdU (magenta), DNA (blue)]. Scale bars, 50 μm. (**B**) Quantification of EdU^{+ve} T47D cells over time. (**C**) Representative images of immunofluorescent staining to evaluate induction of autophagy [autophagic protein (LC3B, green), cytoplasm (F-actin, red), nucleus (DNA, blue), confocal z-stack projections] Scale bars, 50 μm. (**D**) Quantitative analysis of LC3B^{+ve} cells on day 1 and 15 time points with and without treatment. Significant differences were assessed by Student's two-sided *t* test, where differences are shown for comparison between coculture conditions at day 15 time point (*$P < 0.05$, ***$P < 0.001$; full set of *P* values can be found in table S11). Data shown represent the means ± SD ($n = 3$).

formation of dormant single cells or micrometastases for extended periods (*19*, *58*, *61*). Several recent studies also have demonstrated that dormant DTCs use autophagy for prolonged survival in a metastatic site (*28*, *31*, *37*). In this work, we established an approach for probing the influence of soluble secreted factors exchanged between BCCs and BM metastatic niche cells and used this model to understand BCC dormancy/reactivation mechanisms toward improved treatment strategies.

For better understanding ER$^+$ BC DTC dormancy in the BM site, we deployed a NOD-SCID breast cancer dormancy model, where weakly metastatic BCCs were injected intracardially for dissemination and monitored over 6 weeks. We focused on the identification of these DTCs and estimation of their location as they colonize the distant tissue, where they existed as single cells or small micrometastases. Here, we demonstrated that dormant ER$^+$ BC DTCs within the BM were proximate to the bone lining surface, which is known to contain osteoblasts among other bone lining cells. Inspired by these observations, we hypothesized that interactions between osteoblasts and DTCs may be responsible for promoting and sustaining BCC dormancy, with autophagy as a potential dormancy survival mechanism. We examined whether these DTCs were dormant and autophagic by staining for the negative expression of Ki-67 (cell proliferation marker) and autophagy marker LC3B^{+ve}, respectively (Fig. 1B). Observations are consistent with experimental reports of immunostaining studies that suggest that the BM niche promotes DTC dormancy by cell-cell and cell-ECM interactions (*20*, *29*, *32*), including soluble factors (*58*, *60*, *62*), where autophagy is a relevant survival mechanism (*28*, *63*). Direct

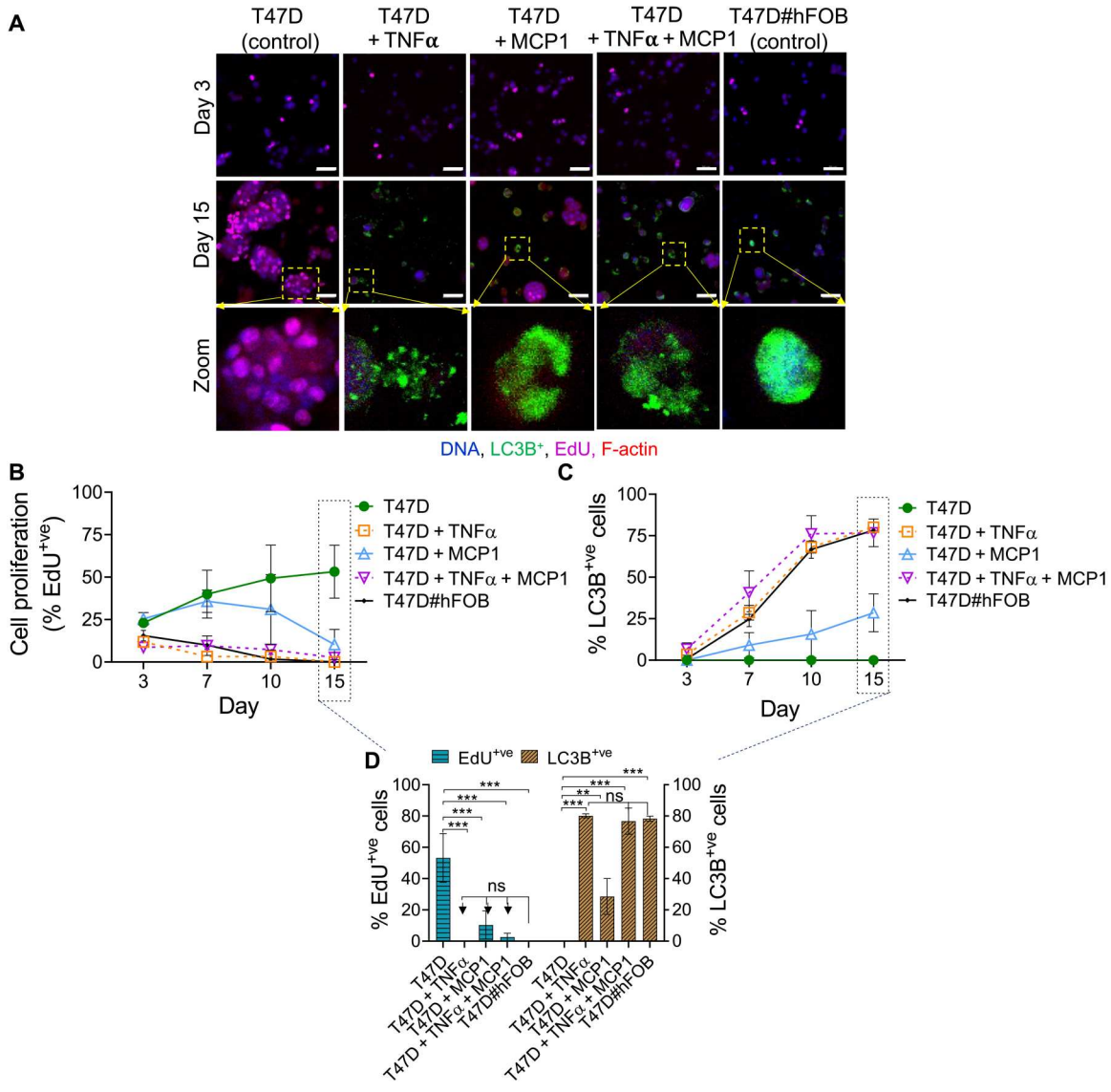

Fig. 9. Probing effects of soluble bioactive proteins on the induction of dormancy and autophagy: Cytokines study. (**A**) Induction of autophagy in different 3D culture conditions with and without treatment of cytokines was assessed by immunofluorescent staining. Representative images of untreated controls or treated monoculture and indirect cocultures [confocal z-stack projections; LC3B (green), F-actin (red), EdU (magenta), DNA (blue)]. Scale bars, 50 μm; additional information in fig. S17. (**B** and **C**) Quantitative analysis of EdU^{+ve} and LC3B^{+ve} puncta cells of T47D in various cultured conditions over time. (**D**) A bar graph of quantification analysis on EdU^{+ve} and LC3B^{+ve} T47D cells at day 15 time points from (B) and (C). Significant differences were assessed by ANOVA with Tukey's multiple comparisons test, where differences are shown for comparison between controls and multiple conditions at day 15 time point (**$P < 0.01$, ***$P < 0.001$; full set of P values for other comparisons can be found in table S12). Data shown represent the means ± SD ($n = 3$). Larger versions of representative images with channels split and zoomed images with scale bars are available in the ESI (fig. S40).

interactions between DTCs and BM niche have been established as important regulators of DTC dormancy: For example, multipotent progenitor cell cannibalism has been demonstrated to promote dormancy (*31*), and specifically, the endosteal niche has been shown to maintain myeloma cell dormancy (*57*).

Building upon these observations, we focused our studies on identifying key indirect cell-cell interactions that regulate ER$^+$ BCC dormancy and reactivation within the BM niche. Several in vivo (subcutaneous tumor model) and in vitro models have been designed to recreate aspects of the BM microenvironment, including the use of bioengineered materials for micrometastases studies (*23*, *62*, *64*). In vitro models also have been used to study interactions between cancer cells and niche cells (*58*, *65*–*67*). The observations made with these in vitro and in vivo model systems highlight the importance of the microenvironment in regulating cancer cell growth at the BM site (*68*, *69*). Yet, challenges have remained in notable a balance between model system complexity, relevance, and reproducibility. For example, for studies of the metastatic cascade, there can be advantages in the use of a model system with increasing complexity (i.e., in vivo models for metastasis studies). However, inherent limitations affect the level of control that can be achieved within these systems, such as limited control

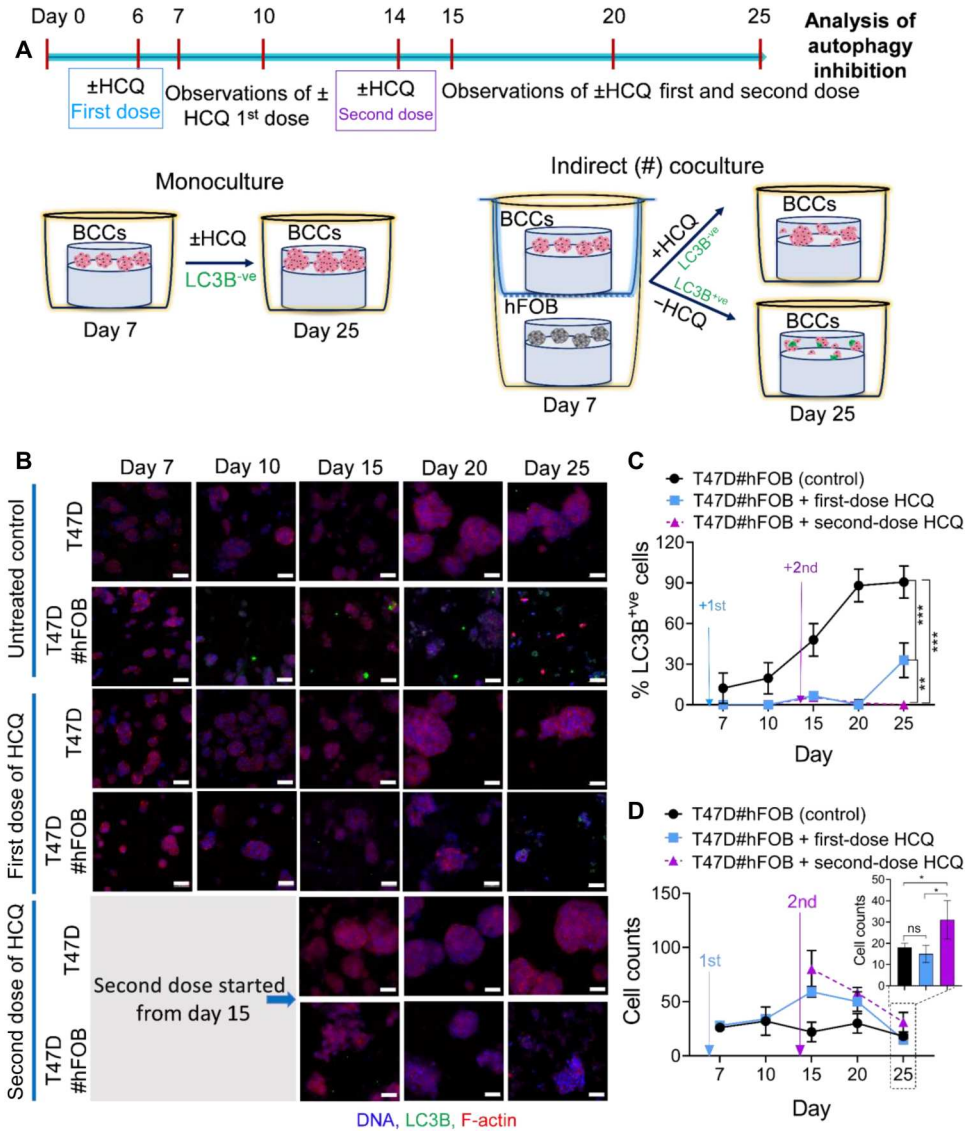

Fig. 10. Dose-dependent response to an inhibitor of autophagy. (**A**) Overview of study for probing effects of inhibition of autophagy over time: HCQ (12.5 μg ml^{-1}) was used as a single dose on day 7, and, for a subset of samples, a second dose was applied on day 15 with continued observation over 25 days for T47D monoculture and T47D#hFOB coculture (control versus treated conditions). (**B**) Representative images of immunofluorescent stained samples probing for autophagy and growth [confocal z-stack projections; LC3B (green), F-actin (red), DNA (blue)]. Scale bars, 50 μm. (**C**) Quantitative analysis of LC3B^{+ve} puncta cells in T47D#hFOB coculture conditions with and without treatment. (**D**) Average number of cells per field of view also was quantified. Significant differences were assessed by ANOVA with Tukey's multiple comparisons test, where differences are shown for comparison between multiple time points (*P < 0.05, **P < 0.01, and ***P < 0.001; full set of P values for other comparisons can be found in table S13). Data shown represent the means ± SD (n = 3).

of specific microenvironment cues, animal-to-animal variations, imaging difficulties, and cost. Consequently, pairing of in vivo and in vitro model systems can prove useful, where in vitro models can be used to reduce some of the complexity of in vivo microenvironments while capturing important cell-to-cell or cell-to-ECM interaction, for both hypothesis-driven studies and the evaluation of therapeutics. Several 3D in vitro culture systems for direct coculture of BCCs and niche cells have been developed in recent years, including the direct culture of BCCs with different BM niche cells in harvested ECMs [e.g., porous collagen scaffolds (*32*), hyaluronic acid (*70*), and niche cell-secreted matrix (*19*, *31*)]. Studies with these systems have provided insights into pivotal direct cell-cell interactions in dormancy/survival/reactivation, including direct BCC-MSC contact (*31*) and the importance of the insoluble ECM proteins produced by niche cells in sustaining BCC quiescence or promoting activation (i.e., dormancy in endothelial-derived thrombospondin 1 within the laminin-rich microvasculature ECM and activation in sprouting neovasculature by periostin and TGF-β1). However, in vitro model systems for studying indirect cell-cell interactions have been limited and are needed for further mechanistic understanding of BCC dormancy and identification and evaluation of therapeutic targets.

Our approach builds upon these prior successes while providing additional levels of controlled complexity. In this work, we

established a well-defined dynamic 3D coculture system that mimics aspects of the complex BM microenvironment for understanding breast cancer dormancy and reactivation mechanism(s) at this site, the most common site of BCC late recurrences (~50% clinical cases) (*1*). ER^+ BCCs with different metastatic potentials (luminal A T47D, luminal A ZR-75-1, and luminal B BT474) were cocultured indirectly with BM niche cells (hMSCs and hFOBs), with each cell type encapsulated within the 3D BM-inspired synthetic matrix and separated using Transwell insert. Our initial studies compared cell responses within the synthetic matrix and in a commercially available harvested collagen matrix in both indirect and direct coculture over 15 days (*30*, *32*). These studies showed similar trends for ER^+ BCCs in both in vitro model systems as follows: (i) BCC growth was inhibited over time when cocultured either directly or indirectly with hFOBs (metabolic activity and % live cells supported), whereas growth was promoted by indirect coculture with hMSCs, relative to monoculture control and direct coculture with hMSCs. (ii) The small clusters of BCCs were viable within indirect (#) hFOB coculture condition over time, and an increase in cluster sizes of BCC was observed with high viability in indirect (#) hMSC coculture condition. These preliminary observations suggested a pronounced response with interactions between BCCs and each BM niche cell type. The persistent single cells and formation of small clusters in vitro in the 3D cocultures with hFOBs within the synthetic matrix were reminiscent of DTCs and micrometastases in vivo. Limited growth and reduced viability, at late times, was observed in both direct and indirect cocultures with hFOBs, suggesting dormancy for the viable BCCs. Direct coculture began with a mixed single-cell suspension of BCCs and niche cells, where interactions would be dominated by distal indirect cell-cell interactions initially, and became increasingly dense as BCC clusters grew for monoculture and hMSC cocultures, with increased proximal indirect cell-cell interactions and direct cell contact. Indirect coculture provided continued separation of BCCs from niche cells over the time course and thus further allowed the parsing of cell responses to indirect interactions in the form of soluble secreted factors. Furthermore, these preliminary studies confirmed that the synthetic matrix was permissive to either BCC growth or dormancy including in response to soluble factors (e.g., growth in monoculture or indirect coculture with hMSCs and dormancy in indirect coculture with hFOBs). Therefore, we continued our studies with only indirect coculture conditions in the well-defined 3D synthetic matrix system.

For probing dormancy, BCC viability and proliferation were initially assessed with a live/dead cytotoxicity assay and subsequently proliferation more directly measured with an EdU assay and immunostaining for proliferation marker Ki-67. Key observations of these studies that included BCCs were viable yet exhibited limited proliferation when cocultured with hFOBs (BCCs#hFOB), suggesting dormancy, and that increased proliferation was observed when cocultured with hMSCs (BCCs#hMSC). The indirect coculture system then facilely allowed us to test the hypothesis that switching from an osteoblastic niche to an hMSC or growth niche promotes BCC reactivation from dormancy, which was achieved by exchanging Transwell inserts from #hFOB to #hMSC or growth media on day 10 followed by culture up to 20 days. BCC switching to proliferation from growth inhibition was observed in these indirect coculture exchange studies and suggested the importance of soluble secreted factors (e.g., cytokines, chemokines, and growth factors) (*45*, *47*) in dormancy/reactivation. In vivo, osteoblasts are known to be critical in both bone homeostasis and repair processes, while MSCs are present in the BM and recruited/expanded in bone injury and remodeling processing (*6*, *34*, *71*): The 3D indirect coculture model provides future opportunities for further capturing and probing these complex interactions in dormancy/reactivation (e.g., tricultures of BCCs, hFOBs, and hMSCs and triggering/examining matrix remodeling).

To further probe the potential mechanism of observed cellular dormancy, we examined autophagy induction in dormant cells within the indirect coculture model, which was observed in vivo and previously reported by others as a potential dormancy survival mechanism (*28*). Among monoculture and coculture conditions, expression of the autophagy marker LC3B was only observed during indirect coculture of BCC in the osteoblastic niche (BCC#hFOB), which was reversed by switching coculture to the MSC niche (BCC#hFOB➔#hMSC at day 10). Our observations of autophagy with dormancy are consistent with recent literature reports: for example, Vera-Ramirez *et al.* (*28*) and Flynn *et al.* (*63*) have shown observed autophagy within the dormant of disseminated murine mammary tumor cells (D2.0R) in lung tissue and in the BM using in vitro (harvested murine BME) and in vivo murine model systems, where autophagy inhibition regulated a dormancy-to-proliferation or dormancy-to-apoptosis switch. Observations of autophagy induction in dormant BCCs within the well-defined 3D indirect coculture model system presented here support its relevance for studies of dormancy/reactivation with insights related to key soluble factors and for targeting dormant cells to prevent a late recurrence. These studies of dormancy used ER^+ cell lines with different metastatic potential, luminal A ZR-75-1 and T47D and luminal B BT474, where all of these cell lines responded similarly under each condition (e.g., exhibiting dormancy in coculture with hFOBs or growth with hMSCs or monoculture). With this confirmation of similarity in responses, we continued further in-depth mechanistic studies with T47Ds, which are routinely used as representative ER^+ BCC line (*72*, *73*) and were observed to form dormant DTCs in vivo, allowing focused in-depth examinations of receptors, proteins, and drug effects.

Next, this robust in vitro model system was used to probe cytokine/chemokine signaling mechanisms where the presence and effects of different soluble factors were examined within the cocultures. We observed that BCC coculture with hFOBs (BCCs#hFOB) resulted in an up-regulation of numerous cytokines, chemokines, and growth factors. Note that the role of inflammation in tumor progression has been controversial; our results are interesting in this context with the observation that TNFα, MCP1, FGF2, and IL-6 among other factors probed were significantly up-regulated in BCCs#hFOB condition relative to monoculture (growth control), which are key factors that have been implicated in dormancy-related BCC responses (*44*, *47*, *50*, *74*, *75*). Identifying dormancy-inducing factors released within the BM niche can guide the design of treatment strategies to target dormant cells. Toward this, we selected two antagonists for receptors (anti-TNFR1 and anti-CCR2) associated with TNFα and MCP1 cytokine/chemokine signaling and examined their ability to prevent BCC induction into dormancy. Results showed blocking for specific receptors and associated signaling with anti-TNFR1 and anti-CCR2 prevented the suppression of BCC growth in the osteoblastic niche (BCCs#hFOB) resulting in BCC proliferation, whereas the untreated dormancy-

promoting coculture condition (BCCs#hFOB; control) maintained limited BCC growth. On the other hand, we separately applied the cytokines/chemokines TNFα and MCP1 to BCCs in monoculture conditions and observed BCC growth suppression and induction of dormancy and autophagy. Overall, these observations support our hypothesis that secreted factors in the BM niche induce BCC dormancy (*44*, *74*, *75*), where TNFR and CCR2 and associated signaling pathways could be potential targets in future studies to prevent disease relapse. Furthermore, we demonstrated how autophagy inhibition with the treatment of HCQ (*76*) could be used to reverse autophagy and induce reactivation of dormant BCCs in the osteoblastic niche with the indirect coculture system. Here, the autophagy inhibition study served both to probe mechanisms and for consideration of autophagy inhibitor dosing regimens that in the future could be considered as part of more complex treatment strategies (e.g., use of autophagy inhibition with other targeted therapeutics to temporarily prevent dormancy and kill proliferating cells that can be further evaluated within in vitro and in vivo models). However, inhibition of autophagy would not be appropriate to consider in the absence chemotherapy or similar treatments aimed at killing growing cancer cells (e.g., early-stage breast cancers treated with only anti-estrogen therapies). Beyond autophagy inhibition, future studies with the model system could evaluate other therapeutic approaches for maintaining dormancy in the presence of reactivating conditions.

Overall, the methods established in and findings of these investigations provide opportunities for improving treatment strategies, including therapeutics for targeting cancer dormancy and innovative systems for these studies. For further mechanistic insights, opportunities for future studies with this system include the examination of cell-cell interactions with increasing complexity and dynamics [e.g., multicellular indirect cocultures of BCCs with hFOBs, hMSCs, and other niche cells (HUVECs), stimulation to mimic injury], examination of paracrine versus autocrine effects (*77*) with nondynamic indirect cocultures, and investigation of synergies between soluble factors and other microenvironment cues (e.g., integrin-binding sites, matrix density, and cell-secreted insoluble factors). For further translational insights, we envision the presented coculture platform being useful in identifying other therapeutics for BCC treatment, testing the utility of a range of therapeutic treatment regimens (e.g., combination therapies, dosing, and duration), and screening of biomarkers for targeting cancer with the potential integration of patient-derived cells.

In conclusion, we used a combination of in vivo and in vitro model systems to probe pivotal indirect interactions between ER^+ BCCs and the BM metastatic niche with mechanistic insights and therapeutic strategies for targeting dormant BCCs. Observations of dormant, autophagic DTCs in the BM proximate to the bone lining in vivo informed design of well-defined 3D indirect coculture systems of BCCs with BM niche cells. A bioinspired synthetic matrix that affords property tuning and reproducibility was implemented as a reduction mimic of the BM tissue within the 3D indirect coculture system, providing control of both cell-matrix and cell-cell interactions. BM niche cells, especially hMSCs and hFOBs, were observed to play a key role in the survival and reactivation of dormant ER^+ BCCs with this system. hMSCs promoted proliferation; hFOBs induced dormancy and autophagy; and switching from hFOB to hMSC or growth conditions promoted reactivation from dormancy. Furthermore, using this indirect hFOB coculture model, we demonstrated that soluble factor signaling associated with TNFR and CCR2 receptors induced dormancy of ER^+ BCCs and survival through autophagy. Targeting of associated pathways (applied antibodies, model drug HCQ) in dormant ER^+ BCCs within the model system further demonstrated the importance of cell-secreted soluble factors in regulating dormancy and the opportunity for treatment strategies by inducing a switch from BCC dormancy to proliferation or death. In summary, we have successfully established a robust 3D indirect coculture model of BCCs with BM niche cells, informed by in vivo observations, for studying key mechanisms of ER^+ BCC dormancy and modulating dormancy/reactivation (fig. S43). This in vitro coculture model could facilitate future exploratory therapeutic screening studies toward preventing ER^+ BCC late recurrence.

MATERIALS AND METHODS

Animal experiments

Animal procedures were conducted by Institutional Animal Care and Use Committee (IACUC) guidelines with the approved protocol (AUP 1311) of University of Delaware (UD), USA. For the distant metastasis of breast cancer, GFP-expressing ER^+ T47D cells (GFP-T47D) [1×10^5 cells in 100 μl of phosphate-buffered saline (PBS)] were injected intracardially into the left ventricle of 6-to-7-week-old female NOD-SCID mice (10 total; Charles River Laboratories) with a 28-gauge needle. A bright red pulse of blood into the syringe was indicated successful insertion into the left ventricle, and the plunger was carefully depressed to inject 100 ml of cell solution without movement of the needle to avoid puncturing the heart. Mice were monitored weekly for any signs of metastatic tumor growth by fluorescence imaging using an IVIS Lumina (UD facility). All mice were euthanized and dissected at 6 weeks after injection. After dissection, all connective tissues were cleaned from the bones (femurs and tibia) and placed in ice-cold PBS, and fluorescence images were captured by IVIS before fixing.

BM tissue fixation and sectioning for characterization of dormant DTCs

Bone tissues (femurs and tibia) were fixed overnight in 4% paraformaldehyde (PFA), which was then replaced with fresh 4% PFA the next day. All bone tissues were decalcified and then embedded in paraffin (by the Histochemistry and Tissue Processing Core facility, Department of Biomedical Research at the Nemours Children's Hospital, Delaware, USA). Whole-mounted bone tissues were sectioned with 5-μm thickness and stained with hematoxylin and eosin, and unstained slices were imaged by a confocal microscope to detect GFP-positive T47D cells (*19*). A set of BM sections were processed for immunofluorescence staining to detect dormant DTCs and identify dormancy mechanisms in the BM site as described below.

Deparaffinization of BM tissue sections for immunofluorescent staining

Paraffin-embedded tissue sections of whole femurs and tibia were deparaffinized in an identical fashion [incubation steps: xylene (5 min); xylene (5 min); 100% ethanol (EtOH) (3 min); 100% EtOH (3 min); 90% EtOH (3 min); 70% EtOH (3 min); deionized water (DiH_2O; Milli-Q, EMD Millipore) (3 min); DiH_2O (3 min)] and then rinsed twice with sterile PBS for 2 × 5 min at room

temperature. Femur or tibia tissue slices were then permeabilized and blocked in a solution containing 1% (w/v) bovine serum albumin (BSA) with 0.05% Triton X-100 in PBS for 2 × 5 min and 3% (w/v) BSA with 0.1% Triton X-100 in PBS for 1 hour at room temperature. After blocking and permeabilization, BM sections were incubated overnight at 4°C in a solution containing 3% (w/v) BSA with 0.05% Triton X-100 in PBS and sequential staining with primary antibody and secondary antibody combinations: rabbit anti-human LC3B (1:500; Novus Biologicals, NB600-1384) overnight incubation followed by washing BM tissue slices [3 × 20 min, 1% (w/v) BSA with 0.05% Triton X-100 in PBS] and then labeling with 1:200 dilution of secondary antibodies (Alexa Fluor 594 goat–anti-rabbit for LC3B, Thermo Fisher Scientific) in blocking solution (2 hours for AF594 and overnight for AF647 at 4°C); subsequently and similarly, rabbit anti-human Ki-67 (1:100; Abcam, ab16667) and 1:200 secondary (Alexa Fluor 647 goat–anti-rabbit for Ki-67, Thermo Fisher Scientific). Tissues were washed thrice with PBS (45 min), incubated with Hoechst 33342 for labeling DNA within cell nuclei (2 μg ml^{-1}, Thermo Fisher Scientific) for ½ hours at room temperature, and washed three times with PBS (45 min) before imaging.

For confocal imaging, each 5-μm-thick section of BM tissue was covered with a coverslip and placed on the confocal microscope (Zeiss LSM 800). Then, the entire BM section (full width and length of the bone) was scanned by generating tile scan sets using four lasers with either 10× or 20× objective, and then regions with observed individual DTCs were imaged with a 20× objective; here, a 100-μm-thick z-stack was used with tile scans to ensure capturing the full section thickness over the entire width and length of the bone section.

ER^+ BCCs and BM niche cell culture and reagents

All ER^+ BCC lines, T47D (HTB-133), ZR-75-1 (CRL-1500), and BT474 (HER2+) (HTB-20), were purchased from American Type Culture Collection (ATCC). BM-derived hMSCs (PT-2501) were purchased from Lonza (Basel, Switzerland). hFOBs (CRL-11372, a human fetal osteoblastic cell line), HUVECs (PCS-100-010, maintained as suggested by ATCC), and human BM stromal cells (HS-5s, CRL-11882) were purchased from ATCC. All cells were grown in Dulbecco's modified Eagle's medium (DMEM)/Hams F-12 50/50 Mix with L-glutamine, 15 mM Hepes (DMEM-F12, Corning cellgro) supplemented with 10% (v/v) fetal bovine serum (Invitrogen), 1% penicillin-streptomycin (PS), 0.2% (v/v) fungizone, and basic FGF (1 ng ml^{-1}) (PeproTech, Rocky Hill, NJ). The culture media were replaced by freshly prepared media every 2 to 3 days, and cells were trypsinized (trypsin/EDTA, Thermo Fisher Scientific) at ~80 to 85% confluency. All BCCs with passages 17 to 25 were used in experiments, and all BM niche cells (hMSCs, hFOBs, HUVECs, and HS-5s) were used before passage 7.

GFP-expressing BCC cell line

ER^+ T47D cells were stably transduced for GFP expression using a commercially available lentiviral system, GFP Control Lentiviral Biosensor from MilliporeSigma (catalog no. 17-10387), per the manufacturer's instructions. Stably transduced cells were isolated using a fluorescence-activated cell sorter (BD FACSAria Fusion High Speed Cell Sorter), passaged multiple times for expansion, and frozen for storage and future use.

For in vivo studies, GFP-expressing ER^+ T47D cells were injected into anesthetized mice for studies of breast cancer dormancy per approved IACUC protocol (AUP no. 1311-2016-0). The use of the stably transduced cell lines enabled in vivo monitoring of tumor growth with the IVIS imaging system (PerkinElmer, IVIS Lumina III) and identification of DTCs in excised tissues. Following the completion of imaging at specific time points during the studies, mice were euthanized, and tissues were removed for histochemical analysis to identify dormant DTCs in particular organs and BM harvested for isolation of dormant DTCs.

3D direct (+) and indirect (#) coculture experiments

All BCCs and BM niche cells were cultured under sterile conditions at 37°C and 5% CO_2 on tissue culture–treated polystyrene flasks (75 and 182 cm^2; CELLTREAT, Pepperell, MA). All cells were grown in DMEM-F12 growth media for use in experiments.

3D culture in collagen scaffolds

A commercially available harvested collagen scaffold (GELFOAM; Pfizer) (*32*) was cut into ~5.5-mm-diameter pieces and ~2.7 mm thick using a sterile biopsy punch and scalpel. All scaffold pieces were washed with sterile PBS for 15 min in a 60-mm petri dish and then placed into an untreated 48-well plate (Chemglass) for monoculture and direct coculture or a 12-well Transwell plate (Corning, 0.4-μm pore size) for indirect coculture experiments. After this, any excess PBS was removed from the scaffold, and then fresh media were applied for another wash before loading the cells. After trypsinization, T47D, hMSC, hFOB, HUVEC, and/or HS-5 cells were deposited as a single-cell suspension for a total cell density of 50,000 cells per each scaffold. For the indirect coculture experiments, scaffolds loaded with BCCs were placed into the Transwell insert, and scaffolds loaded with hMSCs, hFOBs, HUVECs, or HS-5s cells were placed into the well plate below the Transwell insert. For direct coculture experiments, a total of 50,000 cells per collagen scaffold were maintained by evenly splitting among the different cell types seeded. All the plates were sterilely incubated at 37°C and 5% CO_2 for 2 hours to allow complete attachment of cells into the collagen scaffold. DMEM-F12 growth media were then filled in the wells (500 μl per 48-well and 3 ml per 12-Transwell) and transferred into the incubator for analysis at different time points.

Hydrogel preparation for 3D culture

For hydrogel precursor solution preparation, peptides containing alloxycarbonyl (alloc)–protected lysines, K(alloc) that provides a reactive alkene, were synthesized by solid-phase peptide synthesis and characterized using established methods as previously described (*30*, *42*). Briefly, the pendant integrin-binding peptide sequence K(alloc)G$(POG)_3$-PO**GFOGER**G-$(POG)_4$-G (GFOGER) and enzymatically degradable linker peptide K(alloc)G**GPQG↓IWGQ**G-K(alloc) were synthesized using a Liberty Blue Automated Microwave Peptide Synthesizer (CEM, Matthews, NC). The GFOGER sequence was synthesized using a high-swelling ChemMatrix resin (Protein Technologies), and the linker peptide was synthesized on rink amide 4-Methylbenzhydrylamine (MBHA) resin (Novabiochem). For the peptide collection from resin, a cleavage solution was prepared using 95% trifluoroacetic acid (Arcos Organics), 2.5% triisopropylsilane (Arcos Organics), and 2.5% water (all percentages v/v) supplemented with phenol (25 mg ml^{-1}) (Research Products International), and then incubated with a peptide-containing resin for 4 hours. After cleavage from the resin, all peptides

were collected by precipitation in cold diethyl ether (9× excess volume) overnight at 4°C and purified by reverse-phase high-performance liquid chromatography (XBridge BEH C18 OBD 5-μm column; Waters, Milford, MA) with a linear water-acetonitrile (ACN) gradient (water: ACN 95:5 to 45:5; 1.17% change in water per minute). Purified peptides were lyophilized and their molecular weights confirmed via mass spectrometry (*30*). Twenty-kilodalton four-arm polyethylene glycol tetra thiol (PEG-4SH) was either synthesized in the laboratory (*42*) or purchased (JenKem Technology, Plano, TX), breaking any disulfides before use by overnight treatment with tris(2-carboxyethyl)phosphine (350 mg per 1 g of PEG-SH in ≈30 ml) followed by dialysis (molecular weight cutoff of 1 kDa, Spectrum Laboratories, for 24 hours against deionized water at pH 4) and lyophilization. Linker and pendant peptides and PEG-4SH were dissolved in sterile PBS (Invitrogen) supplemented with 1% PS (Invitrogen) and fungizone (0.5 μg ml^{-1}, Invitrogen). Hydrogel precursor solution was prepared by mixing stock solutions for achieving 6% PEG-4SH by weight (wt %), 2 mM pendant peptide, and the balance of linker peptide (1:1 SH:alloc).

3D culture in hydrogels

For 3D culture within hydrogel-based synthetic matrices, ER^+ BCCs (T47D, ZR-75-1, or BT474) and BM niche cells (hMSC or hFOB) were encapsulated either (i) alone for monoculture and indirect coculture (BCCs#hMSC or hFOB) (each BCC line or BM niche cell type individually) or (ii) together (each BCC cell line with respective niche cell type) for direct coculture (BCCs+hMSC or hFOB). First, in preparation for a total volume per hydrogel of 20 μl, 15 μl of the cell-free hydrogel precursor solution was pipetted into a sterile cut syringe (1 ml with the tip removed) and irradiated with cytocompatible doses of light for formation of the hydrogel base bottom layer (10 mW cm^{-2} at 365 nm for 1 min; Inpro Technologies collimating adaptor, Exfo Omnicure Series 2000) (*30*, *42*). Next, a total of 25,000 cells were suspended in 5 μl (5000 cells μl^{-1}) of hydrogel precursor solution, and this suspension was pipetted on top of the previously polymerized 15-μl hydrogel and irradiated with a cytocompatible dose of light (365 nm, 10 mW cm^{-2} for 1 min) to form the cell-laden top layer of the hydrogel (thickness at equilibrium swelling, ~500 μm) on top of the bottom cell-free hydrogel base layer (*30*, *42*); after equilibrium swelling of the hydrogel (V_{eq}/V_{prep} ~ 4), we estimate the density of the cells to be 1250 cells μl^{-1} (1.25×10^6 cells ml^{-1}). For direct coculture, BCCs and BM niche cells were encapsulated at a 1:1 ratio (T47D, ZR-75-1, or BT474+hMSC and T47D, ZR-75-1, or BT474+hFOB) to maintain a total of 25,000 cells per hydrogel replicate. For monoculture or direct coculture, cell-laden hydrogels were placed in a sterile, nontissue culture–treated 48-well plate. For indirect coculture, cell-laden hydrogels with BCCs (T47D, ZR-75-1, or BT474 cells) were transferred into the Transwell insert, and cell-laden hydrogels with BM niche cells (hMSC or hFOB cells) were placed on the bottom of the 12-well Transwell plate. Hydrogels were incubated sterilely at 37°C with 5% CO_2 with 500 μl of growth media overnight followed by a change to fresh growth media. These 3D cultures then were maintained sterilely at 37°C with 5% CO_2 and replacing with media with fresh growth media every 2 to 3 days.

Cell viability

Viability of all BCCs and BM niche cells in collagen scaffolds or hydrogels was determined after 1, 3, 7, 10, and 15 days of culture using a LIVE/DEAD kit (Thermo Fisher Scientific). Briefly, media were removed from the cell-laden constructs (n = 3) followed by washing two times with 300 μl of sterile PBS for 5 min and then incubating with 2 μM calcein acetoxymethyl and 4 μM ethidium homodimer 1 per milliliter solution (in PBS) for 18 min (37°C, 5% CO_2). Before imaging, hydrogels were washed two times in 300 μl of PBS for 5 min and transferred to an eight-well chamber slide (Nunc Lab-Tek II Chambered Coverglass, Thermo Fisher Scientific, Waltham, MA) that was filled with fresh PBS and imaged using a confocal microscope (Zeiss LSM 800, 10× objective and image frame size of 1024 × 1024, 250-μm z-stack, three images per hydrogel sample). Here and in other imaging-based assays, a 250-μm z-stack typically was used to ensure consistent and adequate light penetration through the full thickness of the z-stack for all conditions probed, and no issues were observed with imaging over time (e.g., with different BCC cluster sizes). Orthogonal projections were processed of each z-stack, and live (green) and dead (red) cells were counted using the Volocity software. The percentage of viable cells was calculated using the number of green cells/the total number of (green + red) cells × 100%.

GFP-T47D cells were encapsulated either alone for monoculture or indirect coculture with respective BM niche cells (hFOBs or hMSCs) for direct coculture in hydrogels, or similarly seeded in collagen scaffolds as described in the prior section. Monoculture and direct and indirect coculture were performed as before, and GFP-T47D samples were imaged after 1, 3, 7, 10, and 15 days of culture using a confocal microscope as described for LIVE/DEAD imaging above. The MFI of GFP-expressing T47D cells was measured using the intensity of the green channel from z-stack projections (ImageJ).

Metabolic activity

For 3D cell culture, the metabolic activity of encapsulated cells was measured using AlamarBlue assay reagent (Thermo Fisher Scientific) on days 1, 3, 7, 10, and 15. Briefly, AlamarBlue reagent was diluted 1:10 with phenol red–free DMEM-F12 (Thermo Fisher Scientific) growth media. Then, the media were removed from the wells. All the cultured collagen scaffolds and hydrogels (n = 4 per condition) were transferred to a 48-well plate. After moving, all the samples were incubated with AlamarBlue solution (300 μl per well) for 4 hours at 37°C, 5% CO_2. After this, 100 μl of cultured AlamarBlue solution was collected into a black 96-well plate and the fluorescence intensity measured using a plate reader (BioTek Synergy H4 Hybrid Reader, excitation = 560, emission = 590). Extra cultured AlamaBlue solution was removed from the samples, and indirect cocultured samples were transferred into the previously used Transwell plates and filled with fresh DMEM-F12 growth media.

Cell proliferation assay

Cell proliferation in 3D cultures was assayed using EdU (a thymidine analog) Proliferation Assay Kit AF647 (Thermo Fisher Scientific) at days 3, 7, 10, and 15. Click-iT EdU was used according to the manufacturer′s protocol. Briefly, the conditioned media were removed from the wells, and BCC-laden hydrogels indirectly cocultured with BM niche cells were placed in a 48-well plate. At each time point, BCC-laden hydrogels (monoculture, direct, or indirect culture conditions) were sterilely incubated (37°C and 5% CO_2) with phenol red–free media containing 10 μM EdU solution for 4 hours (300 μl per hydrogel). After the 4-hour incubation, the EdU solution was removed and samples fixed with 4% PFA for

½ hours at room temperature. Then, hydrogels were washed quickly with sterile PBS. A second wash was performed with 1% BSA in PBS and samples were permeabilized with a saponin-based permeabilization solution (300 μl per hydrogel) for 30 min at room temperature. Afterward, samples were incubated with 300 μl of a Click-iT reaction cocktail prepared according to the manufacturer's protocol, with an AF647 azide fluorophore for the copper-catalyzed click reaction 30 min at room temperature (in the dark). Then, samples were washed twice with sterile PBS (2 × 5 min), incubated with Hoechst 33342 (2 μg ml^{-1}, Thermo Fisher Scientific) for ½ hours at room temperature, and washed three times with PBS (45 min) before imaging. The samples were imaged on a confocal microscope (Zeiss LSM 800). Three z-stacks (100 images per stack, 2-μm spacing) were taken per hydrogel (n = 3) for a total of nine images. The quantification analysis of EdU^{+ve} cells was determined by counting the number of EdU cells (AF647)/the total number of cells (Hoechst 33342–stained) × 100% and averaged across replicates (*30*).

For the immunostaining for LC3B after the EdU assay, samples were permeabilized in solution containing 1% (w/v) BSA + 0.0.5% (v/v) Triton X-100 in PBS for 15 min, blocked for 1 hour in 3% (w/v) BSA + 0.1% (v/v) Triton X-100, and then incubated with 1:500 dilution ratio of rabbit anti-human LC3B primary antibody (in PBS) overnight at 4°C. After which, samples were incubated with a secondary antibody, Alexa Fluor 488 goat–anti-rabbit with 1:200 dilution for LC3B staining (Novus Biologicals). The next steps were followed as described in the "Immunostaining of 3D coculture" section.

Luminex multiplex immunoassay

For the Luminex assay, conditioned media were collected from the monoculture or coculture conditions on day 10 before replacing the fresh media and then centrifuged at 3000 rpm for 5 min to remove any cell debris. The supernatant was stored at −80°C until use. Human Magnetic Luminex Assay kit (LXSAHM-09, R&D Systems) containing TNFα, MCP1, FGF2, IL-6, MMP1, and VEGF-A, and EGF was selected as a target inflammatory factor according to breast cancer dormancy and activation relevant signaling in coculture conditions. Before use, frozen media were thawed at room temperature and 50 μl of conditioned media was used (undiluted samples, n = 3) for the sample preparation. Then, levels of cytokines and chemokines were determined using a designed Luminex assay kit according to the manufacturer's protocol. Analyte concentrations were calculated on the basis of standard curves using the xPONENT software (*78*).

Immunostaining of 3D coculture

At each time point, BCC-laden hydrogels were transferred to a 48-well plate and fixed with chilled 4% PFA for ½ hours at room temperature. The samples were washed twice with sterile PBS, and then permeabilized [3% (w/v) BSA + 0.05% (v/v) Triton X-100 in PBS] and blocked [5% BSA (w/v) + 0.1% (v/v) Triton X-100 in PBS], as described earlier. After blocking, hydrogels were incubated with primary antibody (1:500 dilution of rabbit anti-human LC3B, Novus Biologicals) in blocking solution overnight at 4°C. The next day, samples were washed thrice with permeabilization solution (60 min) and incubated overnight with secondary antibody Alexa Fluor 488 goat–anti-rabbit (1:200 dilution; Thermo Fisher Scientific) and phalloidin-TRITC to stain F-actin (1:200 dilution; Sigma-Aldrich) in blocking solution at 4°C. The plate was covered with aluminum foil for protection from light. Then, samples were rinsed (3 × 45 min) with PBS and incubated with Hoechst 33342 (2 μg ml^{-1}, PBS) at room temperature for ½ hours to stain DNA in cell nuclei. The final wash was processed with 3 × PBS (30 min), and samples stored at 4°C in PBS until imaging. As described previously, samples were imaged (n = 3) on a confocal microscope (Zeiss LSM 800). The quantification analysis of $LC3B^{+ve}$ cells and Hoechst-stained nucleus numbers was performed using the Fiji ImageJ software.

For Ki-67 staining, samples were incubated with primary antibody (1:100 dilution of rabbit anti-human Ki-67, Abcam) in blocking solution overnight at 4°C, followed by the steps as described in the first paragraph. The secondary antibody, Alexa Fluor 647 goat–anti-rabbit with 1:200 dilution, was used for Ki-67 staining (Thermo Fisher Scientific).

Cell cycle analysis

Hydrogels were transferred to a microcentrifuge tube and degraded with collagenase (10 U ml^{-1}) (0.5 ml) for 15 to 20 min at 37°C, and any cell clusters were dissociated with Accutase for 10 min at 37°C. The cell suspension was gently mixed after degradation and dissociation. Three gel replicates were pooled per sample and centrifuged at 2000 rpm for 3 min. After removing supernatant, cells were rinsed with PBS (300 μl) and centrifuged. Again, the solution was removed, and cells were fixed with 300 μl of 70% EtOH and transferred overnight to 4°C. The next day, fixing solution was removed, and cells were resuspended with propidium iodide (PI; 1 μg ml^{-1}). Samples were processed on a flow cytometer (Novocyte; Acea Biosciences, San Diego, CA), 10,000 counts per sample, for PI analysis (*42*).

2D cell culture for concentration tests of cytokines and receptor antibodies

ER^+ BCCs or BM niche cells were cultured at a density of 1×10^4 cells per well in triplicate in a tissue culture–treated 96-well plate (Thermo Fisher Scientific). DMEM-F12 growth media were prepared with a stock concentration (100 ng ml^{-1}) with anti-TNFR1 (MAB225-100, R&D Systems), anti–MCP1 receptor (CCR2, 2517/10, R&D Systems), or TNFR1 + CCR2 (1:1 ratio) antibodies, and respective stocks were then diluted on the basis of a dose-dependent test to the cells and incubated for 24 and 48 hours. After which, the plate was processed for AlamarBlue and live/dead assays. The cytotoxic effect of TFNα, MCP1, and TFNα + MCP1 (300-01A and 300-04, PeproTech) cytokine combinations was tested on the T47D cells similarly. The concentrations of respective cytokines or antibodies were chosen for 3D culture experiments on the basis of the 2D culture study, selecting concentrations that were observed to have limited adverse effects on cell viability within the range of those reported in the literature and by the manufacturer to be effective.

Cytokine and chemokine receptor–blocking experiments

Anti-TNFR1 or anti-MCP1 receptor (CCR2) was used to block related signaling including for the cytokine TNFα or chemokine MCP1, respectively. Before cell encapsulation, T47D cells were trypsinized and counted using a hemocytometer. Cells were suspended in fresh DMEM-F12 containing TNFR1, CCR2, or TNFR1 + CCR2 (2 ng ml^{-1}) (1:1 ratio) and incubated for 1 hour at 37°C. After incubation, cell suspensions were centrifuged at 1000 rpm for 5 min

and supernatant was removed. The cell pellet was resuspended in the hydrogel precursor solution for encapsulation. DMEM-F12 growth media supplemented with 2 ng ml^{-1} of each respective antibody were replaced every 2 to 3 days during culture for receptor-blocked cells (*30*, *42*).

Cytokine and chemokine inducing BCC dormancy experiments

ER^+ T47D cells were encapsulated (25,000 cells per gel) in the hydrogel as described previously and placed into a 48-well plate filled with DMEM-F12 growth media with or without of TFNα, MCP1, or TFNα + MCP1 (100 ng ml^{-1}) (1:1 ratio). Fresh media containing TFNα, MCP1, or TFNα + MCP1 (100 ng ml^{-1}) were added to the 3D culture every 2 to 3 days during culture time. The cytokines' effects on T47D cells were analyzed on days 3, 7, 10, and 15 and were compared to controls.

Inhibition of autophagy experiments

HCQ was used as an autophagy inhibitor (Sigma-Aldrich) (*28*). HCQ dose-dependent 2D culture was performed for 24 and 48 hours to observe relevant concentrations within the range of those reported in the literature for suppressing LC3B expression while minimizing cytotoxic effects. T47D cells were seeded at 1×10^4 cells per well in two 96-well plates and grown in DMEM-F12 growth media overnight at 37°C. The next day, a stock solution of HCQ (100 μg ml^{-1}) was prepared, and the dose was applied with serial dilution of 100, 50, 12.5, 6.25, and 3.12 μg ml^{-1} into the well plate and incubated for 24 hours and another one for 72 hours. After incubation, the plate was processed for AlamarBlue and LIVE/DEAD assays and the concentration of 12.5 μg ml^{-1} of HCQ was selected for inhibition of autophagy and use in 3D monoculture and coculture studies.

After cells encapsulation in the hydrogel, 3D monoculture and indirect coculture conditions ($n = 3$) were treated with one or two doses of HCQ solution (12.5 μg ml^{-1}) in growth media at different time points and compared to untreated controls. Hydrogels were processed for immunostaining as described in the immunostaining section and analyzed on days 3, 7, 10, and 15. The quantification analysis was performed using the Fiji ImageJ software.

Statistical analysis

All experiments contained three or more technical replicates, as noted within individual assay sections, and were repeated at least two times (biological replication) to confirm results. Data were analyzed using GraphPad Prism 8. One-way analysis of variance (ANOVA) with Tukey's multiple comparisons test was performed for multiple comparisons, and Student's two-sided *t* test was used when comparing pairwise as noted. All data are expressed as the means ± SE, with replication noted with each specific assay, and statistical significance is denoted as $^*P < 0.05$, $^{**}P \leq 0.01$, and $^{***}P \leq 0.001$.

Supplementary Materials

This PDF file includes:

Figs. S1 to 43
Tables S1 to S13

View/request a protocol for this paper from *Bio-protocol*.

REFERENCES AND NOTES

1. X. H. F. Zhang, M. Giuliano, M. V. Trivedi, R. Schiff, C. K. Osborne, Metastasis dormancy in estrogen receptor–positive breast cancer. *Clin. Cancer Res.* **19**, 6389–6397 (2013).
2. A. F. Chambers, A. C. Groom, I. C. MacDonald, Dissemination and growth of cancer cells in metastatic sites. *Nat. Rev. Cancer* **2**, 563–572 (2002).
3. F. Bray, J. Ferlay, I. Soerjomataram, R. L. Siegel, L. A. Torre, A. Jemal, Global cancer statistics 2018: GLOBOCAN estimates of incidence and mortality worldwide for 36 cancers in 185 countries. *CA Cancer J. Clin.* **68**, 394–424 (2018).
4. S. Braun, C. Kentenich, W. Janni, F. Hepp, J. D. Waal, F. Willgeroth, H. Sommer, K. Pantel, Lack of effect of adjuvant chemotherapy on the elimination of single dormant tumor cells in bone marrow of high-risk breast cancer patients. *J. Clin. Oncol.* **18**, 80–86 (2000).
5. K. Wang, Tumour microenvironment and metastasis, in *Cancer Metastasis* (IntechOpen, 2018).
6. E. Risson, A. R. Nobre, V. Maguer-Satta, J. A. Aguirre-Ghiso, The current paradigm and challenges ahead for the dormancy of disseminated tumor cells. *Nat. Cancer* **1**, 672–680 (2020).
7. C. M. Neophytou, T. C. Kyriakou, P. Papageorgis, Mechanisms of metastatic tumor dormancy and implications for cancer therapy. *Int. J. Mol. Sci.* **20**, 6158 (2019).
8. A. M. Brewster, G. N. Hortobagyi, K. R. Broglio, S. W. Kau, C. A. Santa-Maria, B. Arun, A. U. Buzdar, D. J. Booser, V. Valero, M. Bondy, F. J. Esteva, Residual risk of breast cancer recurrence 5 years after adjuvant therapy. *J. Natl. Cancer Inst.* **100**, 1179–1183 (2008).
9. J. A. Aguirre-Ghiso, Models, mechanisms and clinical evidence for cancer dormancy. *Nat. Rev. Cancer* **7**, 834–846 (2007).
10. O. J. Scully, B. H. Bay, G. Yip, Y. Yu, Breast cancer metastasis. *Cancer Genomics Proteomics* **9**, 311–320 (2012).
11. R. A. Carpenter, J. G. Kwak, S. R. Peyton, J. Lee, Implantable pre-metastatic niches for the study of the microenvironmental regulation of disseminated human tumour cells. *Nat. Biomed. Eng.* **2**, 915–929 (2018).
12. S. Tivari, H. Lu, T. Dasgupta, M. S. De Lorenzo, R. Wieder, Reawakening of dormant estrogen-dependent human breast cancer cells by bone marrow stroma secretory senescence. *Cell Commun. Signal* **16**, 48 (2018).
13. A. Birbrair, *Tumor Microenvironments in Organs* (Springer, 2020), vol. 1296.
14. T. Yoneda, T. Hiraga, Crosstalk between cancer cells and bone microenvironment in bone metastasis. *Biochem. Biophys. Res. Commun.* **328**, 679–687 (2005).
15. M. E. Clements, R. W. Johnson, Breast cancer dormancy in bone. *Curr. Osteoporos. Rep.* **17**, 353–361 (2019).
16. N. D. Walker, J. Patel, K. Guiro, G. Sinha, J. L. Munoz, M. Hu, P. Rameshwar, The bone marrow niche in support of breast cancer dormancy. *Cancer Lett.* **380**, 263–271 (2016).
17. M. S. Sosa, P. Bragado, J. A. Aguirre-Ghiso, Mechanisms of disseminated cancer cell dormancy: An awakening field. *Nat. Rev. Cancer* **14**, 611–622 (2014).
18. C. M. Ghajar, Metastasis prevention by targeting the dormant niche. *Nat. Rev. Cancer* **15**, 238–247 (2015).
19. C. M. Ghajar, H. Peinado, H. Mori, I. R. Matei, K. J. Evason, H. Brazier, D. Almeida, A. Koller, K. A. Hajjar, D. Y. R. Stainier, E. I. Chen, D. Lyden, M. J. Bissell, The perivascular niche regulates breast tumour dormancy. *Nat. Cell Biol.* **15**, 807–817 (2013).
20. P. Carlson, I. M. Coleman, E. T. Goddard, J. Dai, E. M. Schweitzer, A. R. Lim, S. B. Crist, D. A. Cheresh, C. M. Ghajar, Targeting the perivascular niche sensitizes disseminated tumour cells to chemotherapy. *Nat. Cell Biol.* **21**, 238–250 (2019).
21. G. M. Balachander, R. Kotcherlakota, B. Nayak, D. Kedaria, A. Rangarajan, K. Chatterjee, 3D tumor models for breast cancer: Whither we are and what we need. *ACS Biomater Sci. Eng.* **7**, 3470–3486 (2021).
22. S. Pradhan, J. L. Sperduto, C. J. Farino, J. H. Slater, Engineered in vitro models of tumor dormancy and reactivation. *J. Med. Biol. Eng.* **12**, 37 (2018).
23. S. S. Rao, R. V. Kondapaneni, A. A. Narkhede, Bioengineered models to study tumor dormancy. *J. Biol. Eng.* **13**, 3 (2019).
24. R. Korah, M. Boots, R. Wieder, Integrin α5β1 promotes survival of growth-arrested breast cancer cells: An in vitro paradigm for breast cancer dormancy in bone marrow. *Cancer Res.* **64**, 4514–4522 (2004).
25. D. Barkan, H. Kleinman, J. L. Simmons, H. Asmussen, A. K. Kamaraju, M. J. Hoenorhoff, Z. Y. Liu, S. Lockett, C. Khanna, A. F. Chambers, J. E. Green, Inhibition of metastatic outgrowth from single dormant tumor cells by targeting the cytoskeleton. *Cancer Res.* **68**, 6241–6250 (2008).
26. G. Liu, B. Wang, S. Li, Q. Jin, Y. Dai, Human breast cancer decellularized scaffolds promote epithelial-to-mesenchymal transitions and stemness of breast cancer cells in vitro. *J. Cell. Physiol.* **234**, 9447–9456 (2019).
27. W. D. Lu, L. Zhang, C. L. Wu, Z. G. Liu, G. Y. Lei, J. Liu, W. Gao, Y. Hu, Development of an acellular tumor extracellular matrix as a three-dimensional scaffold for tumor engineering. *PLOS ONE* **9**, e103672 (2014).

28. L. Vera-Ramirez, S. K. Vodnala, R. Nini, K. W. Hunter, J. E. Green, Autophagy promotes the survival of dormant breast cancer cells and metastatic tumour recurrence. *Nat. Commun.* **9**, 1944 (2018).
29. L. E. Barney, C. L. Hall, A. D. Schwartz, A. N. Parks, C. Sparages, S. Galarza, M. O. Platt, A. M. Mercurio, S. R. Peyton, Tumor cell–organized fibronectin maintenance of a dormant breast cancer population. *Sci. Adv.* **6**, eaaz4157 (2020).
30. E. M. Ovadia, L. Pradhan, L. A. Sawicki, J. E. Cowart, R. E. Huber, S. W. Polson, C. Chen, K. L. V. Golen, K. E. Ross, C. H. Wu, A. M. Kloxin, Understanding ER+ breast cancer dormancy using bioinspired synthetic matrices for long-term 3D culture and insights into late recurrence. *Adv. Biosyst.* **4**, e2000119 (2020).
31. T. J. Bartosh, M. Ullah, S. Zeitouni, J. Beaver, D. J. Prockop, Cancer cells enter dormancy after cannibalizing mesenchymal stem/stromal cells (MSCs). *Proc. Natl. Acad. Sci. U.S.A.* **113**, E6447–E6456 (2016).
32. R. Marlow, G. Honeth, S. Lombardi, M. Cariati, S. Hessey, A. Pipili, V. Mariotti, B. Buchupalli, K. Foster, D. Bonnet, A. Grigoriadis, P. Rameshwar, A. Purushotham, A. Tutt, G. Dontu, A novel model of dormancy for bone metastatic breast cancer cells. *Cancer Res.* **73**, 6886–6899 (2013).
33. A. D. Kolb, A. B. Shupp, D. Mukhopadhyay, F. C. Marini, K. M. Bussard, Osteoblasts are "educated" by crosstalk with metastatic breast cancer cells in the bone tumor microenvironment. *Breast Cancer Res.* **21**, 31 (2019).
34. R. Dai, M. Liu, X. Xiang, Z. Xi, H. Xu, Osteoblasts and osteoclasts: An important switch of tumour cell dormancy during bone metastasis. *J. Exp. Clin. Cancer Res.* **41**, 316 (2022).
35. B. P. Mahadik, N. A. Bharadwaj, R. H. Ewoldt, B. A. Harley, Regulating dynamic signaling between hematopoietic stem cells and niche cells via a hydrogel matrix. *Biomaterials* **125**, 54–64 (2017).
36. M. A. Ackun-Farmmer, C. A. Soto, M. L. Lesch, D. Byun, L. Yang, L. M. Calvi, D. S. W. Benoit, B. J. Frisch, Reduction of leukemic burden via bone-targeted nanoparticle delivery of an inhibitor of C-chemokine (C-C motif) ligand 3 (CCL3) signaling. *FASEB J.* **35**, e21402 (2021).
37. E. E. Mowers, M. N. Sharifi, K. F. Macleod, Autophagy in cancer metastasis. *Oncogene* **36**, 1619–1630 (2017).
38. N. Linde, G. Fluegen, J. Aguirre-Ghiso, The relationship between dormant cancer cells and their microenvironment. *Adv. Cancer Res.* **132**, 45–71 (2016).
39. Y. Wang, S. Shao, M. Luo, S. Huang, L. Feng, N. Yuan, F. Wu, C. Dang, X. Zhao, Effects of rat bone marrow-derived mesenchymal stem cells on breast cancer cells with differing hormone receptor status. *Oncol. Lett.* **14**, 7269–7275 (2017).
40. M. N. Oliveira, M. M. Pillat, H. Motaln, H. Ulrich, T. T. Lah, Kinin-B1 receptor stimulation promotes invasion and is involved in cell-cell interaction of co-cultured glioblastoma and mesenchymal stem cells. *Sci. Rep.* **8**, 1299 (2018).
41. L. E. Jansen, N. P. Birch, J. D. Schiffman, A. J. Crosby, S. R. Peyton, Mechanics of intact bone marrow. *J. Mech. Behav. Biomed. Mater.* **50**, 299–307 (2015).
42. L. A. Sawicki, E. M. Ovadia, L. Pradhan, J. E. Cowart, K. E. Ross, C. H. Wu, A. M. Kloxin, Tunable synthetic extracellular matrices to investigate breast cancer response to biophysical and biochemical cues. *APL Bioeng.* **3**, 016101 (2019).
43. S. R. Caliari, J. A. Burdick, A practical guide to hydrogels for cell culture. *Nat. Methods* **13**, 405–414 (2016).
44. Y. Yuan, D. Ding, N. Zhang, Z. Xia, J. Wang, H. Yang, F. Guo, B. Li, TNF-α induces autophagy through ERK1/2 pathway to regulate apoptosis in neonatal necrotizing enterocolitis model cells IEC-6. *Cell Cycle* **17**, 1390–1402 (2018).
45. D. Cheleuitte, S. Mizuno, J. Glowacki, In vitro secretion of cytokines by human bone marrow: Effects of age and estrogen status. *J. Clin. Endocrinol. Metab.* **83**, 2043–2051 (1998).
46. J. L. Steiner, E. A. Murphy, Importance of chemokine (CC-motif) ligand 2 in breast cancer. *Int. J. Biol. Markers* **27**, 179–185 (2012).
47. A. S. Khazali, A. M. Clark, A. Wells, Inflammatory cytokine IL-8/CXCL8 promotes tumour escape from hepatocyte-induced dormancy. *Br. J. Cancer* **118**, 566–576 (2018).
48. K. Tasaki, Y. Shintani, T. Saotome, A. Andoh, Y. Fujiyama, S. Hozawa, T. Bamba, Pro-inflammatory cytokine-induced matrix metalloproteinase-1 (MMP-1) secretion in human pancreatic periacinar myofibroblasts. *Pancreatology* **3**, 414–421 (2003).
49. H. F. Dvorak, Vascular permeability factor/vascular endothelial growth factor: A critical cytokine in tumor angiogenesis and a potential target for diagnosis and therapy. *J. Clin. Oncol.* **20**, 4368–4380 (2002).
50. G. Soria, A. Ben-Baruch, The inflammatory chemokines CCL2 and CCL5 in breast cancer. *Cancer Lett.* **267**, 271–285 (2008).
51. Y. Miyamoto, D. L. Hanna, W. Zhang, H. Baba, H.-J. Lenz, Molecular pathways: Cachexia signaling—A targeted approach to cancer treatment. *Clin. Cancer Res.* **22**, 3999–4004 (2016).
52. U. A. Khan, S. M. Hashimi, M. M. Bakr, M. R. Forwood, N. A. Morrison, CCL2 and CCR2 are essential for the formation of osteoclasts and foreign body giant cells. *J. Cell. Biochem.* **117**, 382–389 (2016).
53. S. Gupta, A. Agrawal, S. Agrawal, H. Su, S. Gollapudi, A paradox of immunodeficiency and inflammation in human aging: Lessons learned from apoptosis. *Immun. Ageing* **3**, 5 (2006).
54. S. Mitsuhashi, H. Shima, Y. Li, N. Tanuma, T. Okamoto, K. Kikuchi, M. Ubukata, Tautomycetin suppresses the TNFα/NF-κB pathway via inhibition of IKK activation. *Int. J. Oncol.* **33**, 1027–1035 (2008).
55. W. Xu, Q. Wei, M. Han, B. Zhou, H. Wang, J. Zhang, Q. Wang, J. Sun, L. Feng, S. Wang, Y. Ye, X. Wang, J. Zhou, H. Jin, CCL2-SQSTM1 positive feedback loop suppresses autophagy to promote chemoresistance in gastric cancer. *Int. J. Biol. Sci.* **14**, 1054–1066 (2018).
56. B. A. Virnig, T. M. Tuttle, T. Shamliyan, R. L. Kane, Ductal carcinoma in situ of the breast: A systematic review of incidence, treatment, and outcomes. *J. Natl. Cancer Inst.* **102**, 170–178 (2010).
57. M. A. Lawson, M. M. McDonald, N. Kovacic, W. H. Khoo, R. L. Terry, J. Down, W. Kaplan, J. Paton-Hough, C. Fellows, J. A. Pettitt, T. N. Dear, E. V. Valckenborgh, P. A. Baldock, M. J. Rogers, C. L. Eaton, K. Vanderkerken, A. R. Pettit, J. M. W. Quinn, A. C. W. Zannettino, T. G. Phan, P. I. Croucher, Osteoclasts control reactivation of dormant myeloma cells by remodelling the endosteal niche. *Nat. Commun.* **6**, 8983 (2015).
58. T. T. Price, M. L. Burness, A. Sivan, M. J. Warner, R. Cheng, C. H. Lee, L. Olivere, K. Comatas, J. Magnani, H. K. Lyerly, Q. Cheng, C. M. McCall, D. A. Sipkins, Dormant breast cancer micrometastases reside in specific bone marrow niches that regulate their transit to and from bone. *Sci. Transl. Med.* **8**, 340ra73 (2016).
59. Y. Husemann, J. B. Geigl, F. Schubert, P. Musiani, M. Meyer, E. Burghart, G. Forni, R. Eils, T. Fehm, G. Riethmuller, C. A. Klein, Systemic spread is an early step in breast cancer. *Cancer Cell* **13**, 58–68 (2008).
60. V. Mayhew, T. Omokehinde, R. W. Johnson, Tumor dormancy in bone. *Cancer Rep.* **3**, e1156 (2020).
61. A. C. Yeh, S. Ramaswamy, Mechanisms of cancer cell dormancy—Another hallmark of cancer? *Cancer Res.* **75**, 5014–5022 (2015).
62. H. Peinado, H. Zhang, A. J. Giaccia, I. R. Matei, B. Costa-Silva, M. J. Bissell, S. Hiratsuka, T. R. Cox, C. M. Ghajar, A. Hoshino, G. Rodrigues, B. Psaila, R. N. Kaplan, J. F. Bromberg, Y. Kang, J. T. Erler, D. Lyden, Pre-metastatic niches: Organ-specific homes for metastases. *Nat. Rev. Cancer* **17**, 302–317 (2017).
63. A. L. B. Flynn, B. C. Calhoun, A. Sharma, J. C. Chang, A. Almasan, W. P. Schiemann, Autophagy inhibition elicits emergence from metastatic dormancy by inducing and stabilizing Pfkfb3 expression. *Nat. Commun.* **10**, 3668 (2019).
64. H. Wang, L. Tian, A. Goldstein, J. Liu, H. C. Lo, K. Sheng, T. Welte, S. T. C. Wong, Z. Gugala, F. Stossi, C. Zong, Z. Li, M. A. Mancini, X. H. F. Zhang, Bone-in-culture array as a platform to model early-stage bone metastases and discover anti-metastasis therapies. *Nat. Commun.* **8**, 15045 (2017).
65. P. I. Croucher, M. M. McDonald, T. J. Martin, Bone metastasis: The importance of the neighbourhood. *Nat. Rev. Cancer* **16**, 373–386 (2016).
66. B. Psaila, D. Lyden, The metastatic niche: Adapting the foreign soil. *Nat. Rev. Cancer* **9**, 285–293 (2009).
67. M. T. Haider, D. J. Smit, H. Taipaleenmäki, The endosteal niche in breast cancer bone metastasis. *Front. Oncol.* **10**, 335 (2020).
68. Y. Shiozawa, M. R. Eber, J. E. Berry, R. S. Taichman, Bone marrow as a metastatic niche for disseminated tumor cells from solid tumors. *Bonekey Rep.* **4**, 689 (2015).
69. S. Liu, C. Ginestier, S. J. Ou, S. G. Clouthier, S. H. Patel, F. Monville, H. Korkaya, A. Heath, J. Dutcher, C. G. Kleer, Y. Jung, G. Dontu, R. Taichman, M. S. Wicha, Breast cancer stem cells are regulated by mesenchymal stem cells through cytokine networks. *Cancer Res.* **71**, 614–624 (2011).
70. A. A. Narkhede, J. H. Crenshaw, R. M. Manning, S. S. Rao, The influence of matrix stiffness on the behavior of brain metastatic breast cancer cells in a biomimetic hyaluronic acid hydrogel platform. *J. Biomed. Mater. Res. A* **106**, 1832–1841 (2018).
71. A. A. Al-Bari, A. Al Mamun, Current advances in regulation of bone homeostasis. *FASEB Bioadv.* **2**, 668–679 (2020).
72. S. Yu, T. Kim, K. H. Yoo, K. Kang, The T47D cell line is an ideal experimental model to elucidate the progesterone-specific effects of a luminal A subtype of breast cancer. *Biochem. Biophys. Res. Commun.* **486**, 752–758 (2017).
73. D. L. Holliday, V. Speirs, Choosing the right cell line for breast cancer research. *Breast Cancer Res.* **13**, 215 (2011).
74. A. M. Mastro, C. V. Gay, D. R. Welch, H. J. Donahue, J. Jewell, R. Mercer, D. DiGirolamo, E. M. Chislock, K. Guttridge, Breast cancer cells induce osteoblast apoptosis: A possible contributor to bone degradation. *J. Cell. Biochem.* **91**, 265–276 (2004).
75. J. Harris, Autophagy and cytokines. *Cytokine* **56**, 140–144 (2011).
76. J. Lorente, C. Velandia, J. A. Leal, Y. Garcia-Mayea, A. Lyakhovich, H. Kondoh, M. E. LLeonart, The interplay between autophagy and tumorigenesis: Exploiting autophagy as a means of anticancer therapy. *Biol. Rev.* **93**, 152–165 (2018).

77. M. Esquivel-Velazquez, P. Ostoa-Saloma, M. I. Palacios-Arreola, K. E. Nava-Castro, J. I. Castro, J. Morales-Montor, The role of cytokines in breast cancer development and progression. *J. Interferon Cytyokine Res.* **35**, 1–16 (2015).
78. L. A. Sawicki, L. H. Choe, K. L. Wiley, K. H. Lee, A. M. Kloxin, Isolation and identification of proteins secreted by cells cultured within synthetic hydrogel-based matrices. *ACS Biomater Sci. Eng.* **4**, 836–845 (2018).

Acknowledgments: We would like to thank the laboratory of K. Lee especially L. Choe for access to Luminex; the laboratory of W. Chen for access to plate reader; Histochemistry and Tissue Processing Core Lab of Nemours Biomedical Research for tissue sectioning; and the UD Office of Laboratory Animal Medicine (OLAM) for IVIS and animal facility access. **Funding:** This work was supported by a grant from the Susan G. Komen Foundation (CCR16377327) made possible by funding from American Airlines, as well as an NIH Director's New Innovator Award (DP2 HL152424-01) for related research. Fellowship support for D.M. was provided in part by the National Institute of General Medical Sciences (NIGMS) of the NIH under award number T32GM133395. Facilities and instrumentation were supported by an Institutional Development Award (IDeA) for a Center of Biomedical Research Excellence (COBRE) from the NIGMS within the NIH (P20GM104316 and P20 GM103446) and by the NSF through the University of Delaware Materials Research Science and Engineering Center (DMR-2011824). **Author contributions:** L.P., R.A.S., K.v.G., and A.M.K. conceived the ideas and designed the study. L.P. and E.M.O. synthesized and characterized materials and developed EdU protocol. L.P. performed 2D and 3D culture studies. D.M. performed 2D culture studies. L.P. and T.C. performed in vivo studies. S.L.S. performed rheometry studies. L.P. analyzed the data and prepared all figures. R.A.S., L.P., and A.M.K. developed animal protocol. R.A.S. performed training on intracardiac injection. L.P., D.M., and A.M.K. wrote the manuscript with contributions from all coauthors. **Competing interests:** L.P., D.M., R.A.S., K.v.G., and A.M.K. acknowledge the submission of a patent application related to the work (application no. 17/764,593; filing date 29 March 2022). The other authors declare that they have no competing interests. **Data and materials availability:** All data needed to evaluate the conclusions in the paper are present in the paper and/or the Supplementary Materials.

Submitted 17 August 2022
Accepted 3 February 2023
Published 8 March 2023
10.1126/sciadv.ade3186

ScienceAdvances

Dynamic bioinspired coculture model for probing ER+ breast cancer dormancy in the bone marrow niche

Lina Pradhan, DeVonte Moore, Elisa M. Ovadia, Samantha L. Swedzinski, Travis Cossette, Robert A. Sikes, Kenneth van Golen, and April M. Kloxin

Sci. Adv., **9** (10), eade3186.
DOI: 10.1126/sciadv.ade3186